UPPSALA
UNIVERSITET

Digital Comprehensive Summaries of Uppsala Dissertations from the Faculty of Science and Technology 641

Acoustic Manipulation of Particles and Fluids in Microfluidic Systems

LINDA JOHANSSON

ACTA
UNIVERSITATIS
UPSALIENSIS
UPPSALA
2009

ISSN 1651-6214
ISBN 978-91-554-7513-0
urn:nbn:se:uu:diva-100758

Dissertation presented at Uppsala University to be publicly examined in Seigbahnsalen, Ångström laboratories, Regementsv. 1, Uppsala, Friday, May 15, 2009 at 13:15 for the degree of Doctor of Philosophy. The examination will be conducted in English.

Abstract
Johansson, L. 2009. Acoustic Manipulation of Particles and Fluids in Microfluidic Systems. Acta Universitatis Upsaliensis. *Digital Comprehensive Summaries of Uppsala Dissertations from the Faculty of Science and Technology* 641. 81 pp. Uppsala. ISBN 978-91-554-7513-0.

The downscaling and integration of biomedical analyses onto a single chip offers several advantages in speed, cost, parallelism and de-centralization. Acoustic radiation forces are attractive to use in these applications since they are strong, long-range and gentle. Lab-on-a-chip operations such as cell trapping, particle fluorescence activated cell sorting, fluid mixing and particle sorting performed by acoustic radiation forces are exploited in this thesis. Two different platforms are designed, manufactured and evaluated.

Keywords: acoustic manipulation, bioanalysis, cell sorting, cell trapping, piezoelectric

Linda Johansson, Micro Structural Technology , Department of Engineering Sciences, Box 534, Uppsala University, SE-75121 Uppsala, Sweden

ISSN 1651-6214
ISBN 978-91-554-7513-0
urn:nbn:se:uu:diva-100758 (http://urn.kb.se/resolve?urn=urn:nbn:se:uu:diva-100758)

List of papers

Paper I *An Evaluation of the Temperature Increase from PZT Micro-Transducers for Acoustic Trapping,*
L. Johansson, M. Nilsson, T. Lilliehorn, M. Almqvist, J. Nilsson, T. Laurell, S. Johansson, *Conference Proceedings IEEE Ultrasonics 2005, 1614-1617*

Paper II *Noninvasive Acoustic Cell Trapping in a Microfluidic Perfusion System for Online Bioassays*,
M. Evander, L. Johansson, T. Lilliehorn, J. Piskur, M.Lindvall, S. Johansson, M. Almqvist, T. Laurell, J. Nilsson, *Analytical Chemistry, 2007, 79, 2984-2991*

Paper III *Temperature control and resonance mode analysis of an acoustic trap for μTAS*,
L. Johansson, M. Nilsson, T. Lilliehorn, M. Almqvist, J. Nilsson, T. Laurell, S. Johansson, submitted to *Ultrasonics*

Paper IV *Effective mixing of laminar flows at a density interface by an integrated ultrasonic transducer,*
L. Johansson, S. Johansson, F. Nikolajeff, S. Thorslund, *Lab on a Chip, 2009, 9, 297-304*

Paper V *On-chip fluorescence activated cell sorting by an integrated miniaturized ultrasonic transducer*,
L. Johansson, F. Nikolajeff, S. Johansson, S. Thorslund, accepted for publication in *Analytical Chemistry*

Paper VI *Surface Acoustic Wave-induced particle sorting with node-position flexibility*,
L. Johansson, J. Enlund, S. Johansson, I. Katardjev, V. Yantchev, submitted to *Lab on a Chip*

Paper VII *Surface Acoustic Wave-induced particle manipulation in a glass microfluidic channel*,
J. Enlund, L. Johansson, S. Johansson, I. Katardjev, V. Yantchev, submitted to *Journal of Micromechanics and Microengineering*

Paper VIII *Acoustic manipulation of sub-micrometer particles by interface waves in microfluidic channels,*
V. Yantchev, J. Enlund, S. Johansson, I. Katardjev, L. Johansson, submitted to *Lab on a Chip*

Author's contribution to the publications

Paper I Joint planning. Major part of manufacturing, evaluation, analysis and writing.

Paper II Minor part of manufacturing, evaluation, analysis and writing.

Paper III Joint planning. Major part of manufacturing, evaluation, analysis and writing.

Paper IV Joint planning, manufacturing and evaluation. Major part of analysis and writing.

Paper V Joint planning, manufacturing, evaluation and writing. Major part of analysis.

Paper VI Joint planning, manufacturing and analysis. Major part of evaluation and writing.

Paper VII Joint planning, manufacturing, analysis and writing. Major part of evaluation.

Paper VIII Joint planning, manufacturing and analysis. Major part of evaluation. Minor part of writing.

Patent applications

US 12/198642 Particle Sorting

Contents

Abbreviations

LOC	lab on a chip
POC	point of care
μTAS	micro total analysis system
MST	microstructure technology
BAW	bulk acoustic wave
SAW	surface acoustic wave
IAW	interface acoustic wave, also Stonley wave
IDT	interdigital transducers
MIT	miniaturized integrated transducers
FACS	fluorescence activated cell sorting
FFF	field flow fractionation
FEM	finite element method

1 Introduction

The Lab-On-a-chip (LOC) technology represents a revolution in laboratory experimentation, with numerous applications in genomics, proteomics and cellomics, in point-of-care systems and in in-the field warfare detection. The research in this field has since 1990 resulted in a toolbox of techniques available to perform a number of desired unit operations. The scope of this thesis has been to exploit acoustic manipulation in the field of LOC. Two fundamental designs are evaluated and several different operations are demonstrated. The unit operations evaluated in this thesis are cell trapping, sorting of single cells by fluorescence activation, non-labeled sorting of particles from the medium and fluidic mixing.

1.1 Downscaling and Integration

In the field of 'lab-on-a-chip' (LOC) bioanalytical systems are scaled down and integrated onto a single chip, 'micro Total Analysis Systems' (μTAS), *Figure 1-1*. In addition to scaling down the large scale methods, new methods only applicable in the micro-scale régime are employed.

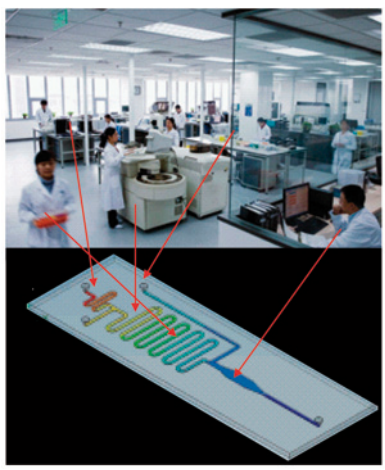

Figure 1-1. In LOC-systems several bio-analytical operations are miniaturized and integrated onto a single chip. (*Courtesy of MDS Pharma Services and Micronit Microfluidics.*)

All the following general motivations for LOCs are relevant for some or all the papers included in the thesis.

1.1.1.1 Speed and cost

Miniaturization offers several advantages compared with conventional equipment such as:

- Enables integration of several steps which speeds up analysis time by eliminating the labor for transferring the sample from one station to the next.
- Less sample volume is required and for instance a single drop of blood can be enough for the analysis.
- Evaluations of many combinations can be performed in a short time in systems with high degree of parallelism, such as for drug discovery.
- The amount of costly reagents can be decreased which decreases the overall cost.
- The short distances in small volumes speed up reactions.
- Thermal management can also be performed faster which also increases the reaction speed.
- For large-scale applications, the manufacturing cost can be low by the use of mass-fabrication process technology.

An example of a method that benefits from downscaling is the polymer chain reaction method (PCR) where DNA is magnified by heat cycling. Another method is capillary electrophoresis (CE) for the detection of proteins, peptides or DNA based on charge. In 2002, DNA analysis was the most studied technique at the microscale, next to CE.[1]

1.1.1.2 Parallelism

The integration of several unit operations into the same system minimizes the risks of handling infectious samples by the elimination of transfer steps. Furthermore, the high degree of parallelism possible in microfluidics, enables addressing more complex questions in proteomics, genomics and cellomics.

In gene and protein assays, the presence of specific genes or proteins in the sample is evaluated through DNA-hybridization or antibody-antigen interactions. Miniaturizing of the micro-titer 96-well plates into 2D arrays, *Figure 1-5C*, enabled increase in speed and parallelism of the assays.

In cellomics, flow cytometry equipment enables single-cell analysis of cells in a stream, such as in Fluorescence activated cell sorters (FACS). The study of single cells attracts special attention since the diversity of a colony of cells makes it difficult to relate the response to a certain stimuli.[2] Additionally, the integration of multiple culturing regions in cellomics enables co-culturing of cells to study their relative interaction, which is applicable for instance for artificial organs systems, e.g. liver cells.[3]

1.1.1.3 Controlled microenvironment

The fact that LOC systems are in the same scale as cells, as well as the ability to provide precise control of the chemical and physical environment in microsystems, offers new possibilities for cellomics. As opposed to the traditional platforms of micro-titer plates, microfluidic systems enable more *in vivo*-like properties of volume flows and of the ratio of culture media to cell volume.[4] Concentration gradients which control many cell responses, such as axonal growth, can be created in microfluidic systems.[5]

1.1.1.4 Point-of-care

Due to small size and low cost, LOC systems can be used at local health centers instead of at large hospitals, or by the patient herself at home instead of in an analysis lab. Such decentralized systems are called Point-of-Care (POC) systems. Desired POCs are for use in malaria tests, HIV tests, as inflammatory markers, in cancer diagnosis, and in the detection of anabolic steroids and allergies. The portability of POC systems is emphasized for warfare detection systems to enable early warnings of explosives, toxins or pathogens. POC systems are often disposable in part or as a whole, and are therefore required to operate without expensive and bulky pumping systems and signal read-out instrumentation. Additionally, the systems should be possible to operate without specially trained personnel.

1.1.2 Microfluidics in academia

The term μTAS was coined in 1990[6], in an article were many of the advantages expected for miniaturized analyzes were outlined. The term LOC was introduced later to include other processes than only analysis and the term microfluidics is today used in equivalence. Four factors played an essential role for the realization of LOC; applications in analytical chemistry, the advances in genomics in the 1970-1980, the fear of terror in the 1980ies and the processing toolbox developed in the microelectronics and the microstructure technology (MST) from the 1960ies until today. As can be seen from *Figure 1-2* the field has grown exponentially over the last decade.

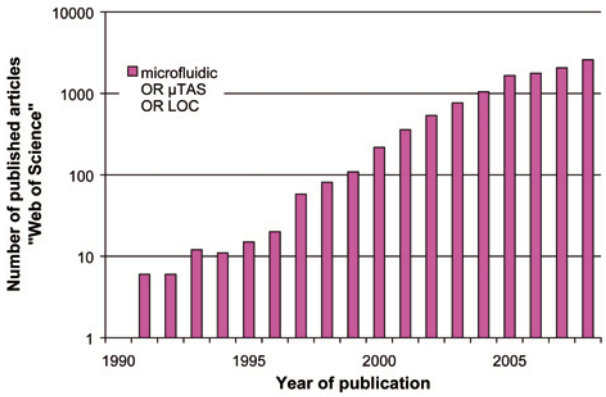

Figure 1-2. A rough estimate of the number of journal articles published since 1990 as determined by using a simple keyword search (Microfluidic + Lab on a Chip + micro total analysis system) in *Web of Science*.

1.1.3 Microfluidics in industry

Some of the more important microfluidic platforms[7] are shown in *Figure 1-3*, all of which have commercial exploitation. These systems provide a number of unit operations, such as flow transport, fluid metering, fluid valving, mixing, separation, concentration, and detection.

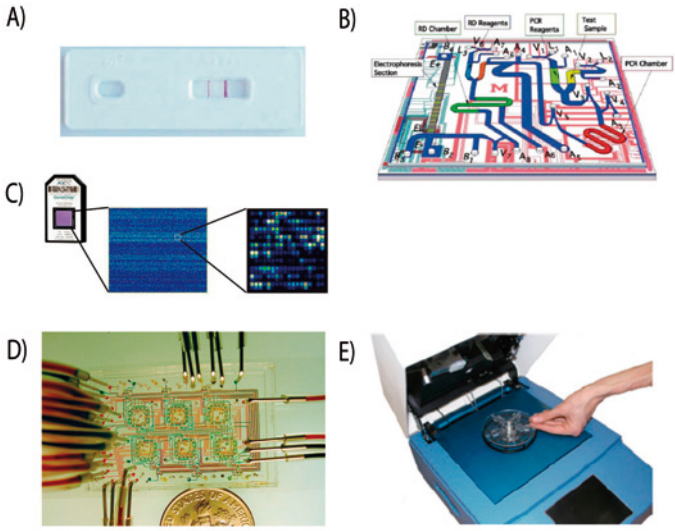

Figure 1-3. Illustrations of the most important LOC-platforms (A) dip-stick with capillary driven flow, (B) the electrophoresis platform with EOF-driven flow,[8] *(Reproduced by permission of the Royal Society of Chemistry*) (C) the microarray-platform,[9] (D) the pneumatic driven and valving platform, from[10] (*Reprinted with permission from AAAS.*), (E) the centrifugal platform[11] (*Reproduced by permission of the IOP*).

1.2 The microfluidic domain

The term microfluidics is generally used for microscopic and nanoscopic volumes in 10-100 µm wide channels. In this micro-scale domain, the physical properties obtained for fluidics are different than in the large scale. The main characteristic is that viscous forces are significant in relation to inertial forces and therefore the fluid behaves in a more orderly fashion. Due to this *laminar flow* property, it is possible to predict the position of a fluid segment at a later time. Another consequence of laminar flow is that mixing between fluids, which is an operation commonly preformed in analysis, does not occur in a straight channel and must be actively mediated. In *Paper 4*, the mixing of fluids by radiation forces was demonstrated. Not only flow properties are different in the microfluidic domain. For instance, surface properties dominate over volume forces such as gravity. Microfluidic equations are found in *Appendix A*.

The laminar property of the fluid makes it applicable for flow simulations of the Navier-Stoke's equation. Trajectories of particles in the flow is modeled in Finite Element Method (FEM) analysis, *Figure 1-4*, for the flow split outlet design used in *Paper 6*, and for a multiple outlet design that can be employed for acoustic Field Flow Fractionation[12] (see 1.3). Forces acting on particles in a flow, such as Stokes drag force and buoyancy-corrected gravitational force are described in *Appendix A*.

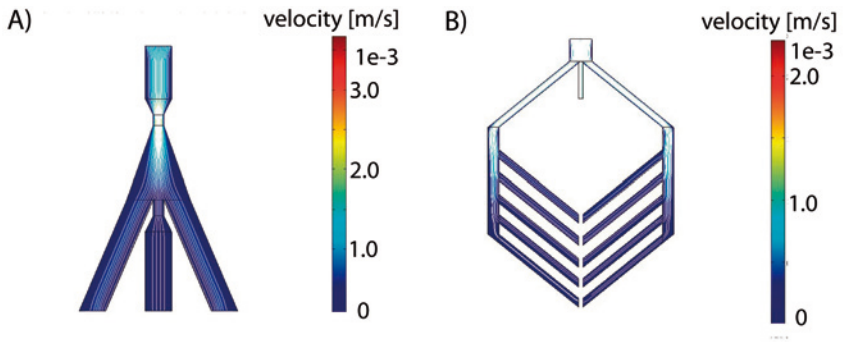

Figure 1-4. Flow-split design: A) for sorting the particles in a small part of the middle flow by a modified trifurcation outlet, *Paper 6*, and B) for simultaneous separation of several particles into multiple outlets depending on their lateral position in the channel. Finite element method (FEM) simulation (Comsol Multiphysics AB) of the flow velocities and the particle trajectories (white lines).

1.3 Continuous-flow systems

Continuous-flow systems is an important group of LOC and have applications in cell-culturing during continuous perfusion, *Paper 1-3,* and for cell separation, *Paper 5-8*. The flow is generally driven by a syringe pump. Real-time studies on trapped cells can be performed and the effect of concentration gradients can be evaluated. The continuous flow operation enables addition of fresh nutrients and removal of harmful bi-products. For trapping in multiple spots tracking of a population of single cells over time is possible.[13]

Ultrasound in continuous flow has been used to achieve a 2D trapping zone.[14, 15] In comparison with a flat surface, a 2D or a 3D zone better mimics the *in vivo* conditions of animal cells.[16] For separation of cells, the benefits of continuous flow compared to batch operation are the integration with other steps and the possibility to adjust parameters during the operation.[17]

Flow cytometry equipment operates in continuous flow and has been the standard metrology for quantitative analysis of cell populations for the past 20 years.[18] It offers single-cell analysis of a cell population at a specific point in time. A flow cytometer that also sorts a selected part of the sample is the Fluorescence Activated Cell Sorter (FACS), *Figure 1-5A*. The miniaturization of FACS is an active research field, and was the application for the device in *Paper 5*. Continuous-flow sorting of several type of particles into multiple outlets can be performed by Field Flow Fractionation (FFF),[19] *Figure 1-5B,* by applying a gradient force perpendicular to the flow. Examples of these systems include posts for size-selective sorting,[20] pinched-flow-fractionation,[21] dielectrophoretic forces[22] and acoustic forces[12].

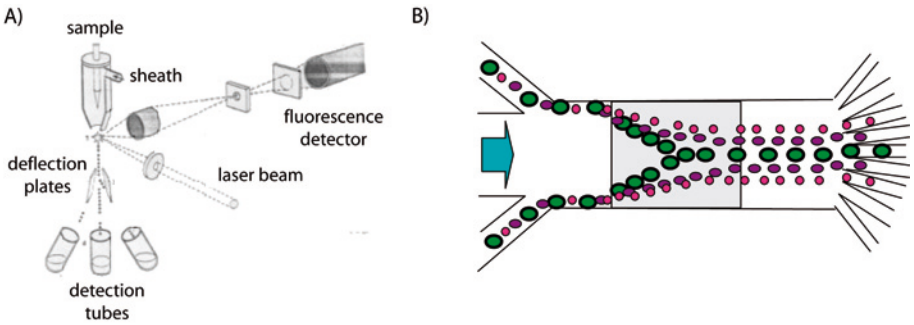

Figure 1-5. Examples of continuous-flow devices: (a) single-cell separation in a Fluorescence Activated Cell Sorter (FACS) and (b) Field flow fractionation (FFF) cell-sorting by acoustic forces.[12] In the FACS, the cells are enclosed in a droplet of sheat water at the tip of a container and dispensed into air by a piezoelectric transducer. A charge is applied to the surface of the drop and depending on the fluorescent signal the drop is deflected by the electrostatic interaction at the deflector plates and collected in one of several outlets.

1.3.1 Beads and droplets

For the evaluation of sorting or trapping devices, beads can be used to mimic cell behavior. Coated bead surfaces can also be used in assays as sites for reactions to take place since they offer large area that interacts with the sample. A common assay is the enzyme-linked immunosorbent assay (ELISA) where occurrence of an analyte in the sample generates the binding of two beads with different surface coatings. Another method is the latex agglutination test (LAT), where the molecule of interest binds to the surfaces of several beads which then forms a cluster. The cluster can be detected by the naked eye and its size is a measure of the analyte concentration. The method is less sensitive than ELISA and is employed for instance in quantitative dipstick pregnancy tests.

Furthermore, the mobility of beads enables exposure to a larger part of the sample volume thereby increasing the rate of reaction. Moreover, beads can be separated from the sample before detection, leading to lower background noise. Additionally, the beads can be used to remove some component in the sample, such as for magnetic beads which are used in several commercial systems.

Droplets can be used as individual compartments in continuous flow. For instance, gel spherulites are used to enclose molecules exerted from a cell in low concentration.[23] Gel encapsulation beads can mimic 3D *in vivo* conditions and can be used for instance during transplantation to aid clusters of cells in withstanding physical barriers.[24]

1.4 Downscaling and Integration – general challenges

Signal detection and sample preparation are two steps that impose challenges in LOC systems. Fluorescence detection is a common technique for signal detection, either by incorporating fluorescent dye into the bead material or for cells by modifying the genome of the cell to express for instance the green fluorescent protein (GFP)[a]. The fluorescent signal is proportional to the transmitting volume and hence decreases with smaller sizes. Sensitivity, however, increases by down-scaling since the background noise is proportional to the detection volume.

Other signal detection methods include detection by impedance in a Coultier Counter. This technique is less diverse than fluorescence detection but does not require labelling. Electrochemical detection methods scale better with decreasing sizes,[25] but their sensitivity is inferior to fluorescence. For detection of small molecules onto surfaces, mass-loading probes, such as

[a] which discovery was awarded with the Nobel Prize in chemistry 2008

Quartz Crystal Microbalance (QCM) or Surface Plasmon resonance (SPR), can be used.

Sample preparation is often a challenging task and is often performed off-chip. The steps that are performed can be dilution, separation and extraction, in addition to introduction of buffer media or growth media.

In addition to solving the bottle-neck steps of detection and sample-preparation, Whitesides requested in 2006 a 'killer application' that would pay a disproportionally large part of the cost of the introduction of a new technology to speed up the commercialization of LOCs.[26] He did foresee such applications, however, requiring simultaneous innovations in biomedicine as well as microfluidics. Examples of such applications are for monitoring patient response to therapy, and for anticipating disease by early detection of biomarkers for home testing and for tests at the doctor's office.

1.5 Micro Structure Technology (MST) and 'fine mechanics'

The fabrication of the microfluidic platforms are made by microstructure technology (MST). Additive methods (such as metal evaporation and sputtering or polymer spinning) and subtractive methods (such as dry or wet etching) are performed on planar surfaces. An essential step is called lithography in which a pattern is transferred from a mask to a substrate. It is performed by deposition of a photo-sensitive polymer onto a substrate which is subsequently illuminated by UV-light through a mask which contains the pattern. The UV-light either strengthens or weakens the exposed parts and upon immersing the substrate into a developer, the weak part of the polymer is dissolved and the pattern is transferred to the surface. The small scale features usually requires processing clean room facility.

MST-techniques were initially developed for the microelectronics industry. Extending these processing techniques to also include structural components approaching the 3D, signifies the field of microstructure technology (MST). Since many of the devices manufactured were sensors and actuators, the field is often called microelectromechanical system (MEMS).

Silicon is often used as the structure material due to the process knowledge developed in microelectronics, as well as its mechanical properties. Polymers are also used as structural material, and offer low cost mass-fabrication, fast reproduction, optical transparency and flexibility with regard to the mechanical properties. Structuring of polymers can sometimes be performed by etching and lithography, but more often other techniques such as casting or injection molding are used. In microfluidics, glass is another common structuring material, due to its electrical, mechanical and surface properties.

Manufacturing techniques labeled ‘fine mechanics’ such as milling, drilling and pick-and-place assembly are often employed in addition to MST.

1.6 LOC systems in this thesis: Miniaturized Integrated Transducer (MIT) and Inter Digital Transducer (IDT)

Two types of transducers are used to excite the acoustic signal in this thesis: Miniaturized Integrated Transducers (MIT) and Inter Digital Transducer (IDT), *Figure 1-6.*

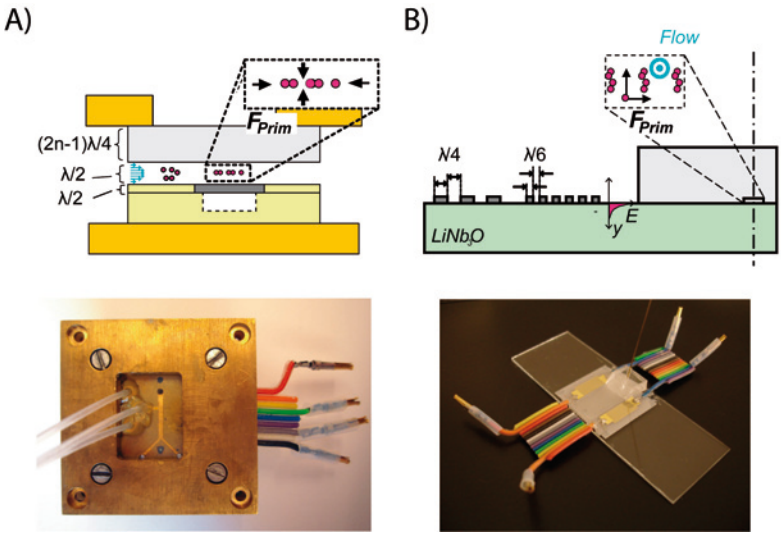

Figure 1-6. Illustration and photographs of A) the Miniaturized Integrated Transducer (MIT) platform and B) the Inter Digital Transducer (IDT) platform.

The work on these platforms in this thesis is summarized as follows:

- MITs of different piezoelectrical materials were evaluated in terms of temperature increase and acoustic output *Paper 1*. An MIT platform was evaluated for cell assays, *Paper 2*, in terms of trapping force for single-bead, viability and temperature increase at resonance as a function of driving voltage. In *Paper 3* the optimal driving frequency regarding temperature increase and trapping efficiency was evaluated and a 1D-modell employed.
- In *Paper 4* a novel method for generating mixing at a density interface by acoustic radiation forces was demonstrated and modeled.
- Particle sorting at a density interface for application in µFACS was demonstrated in *Paper 5*.

- In *Papers 6-8* Interdigital transducers (IDTs) and surface acoustic waves (SAW) are employed instead of bulk acoustic waves (BAW) for excitation of the acoustic wave. In *Paper 6* the channel is made of PDMS and in *Paper 7* a glass channel is used. In *Paper 8* the selection of channel and piezoelectric material and the propagation direction allows for coupling of the SAW into the channel by interface acoustic waves (IAW), and the manipulation of small polystyrene particles (0.5 μm diameter) was demonstrated.

2 Manipulation of particles or fluids by acoustic forces

Acoustic forces can be exploited for several μTAS operations, such as trapping of particles, separation of different type of particles, alignment of particles before detection or sorting, enrichment of particles, purification of fluid and mixing of fluids. The term particle refers to a cell or a bead. Three effects of the acoustic field are generally considered: acoustic radiation force, acoustic streaming and acoustic cavitation.

Acoustic particle manipulation is generally performed by the acoustic radiation force. The origin is a difference in momentum flux, for instance between two interfaces. Acoustic mixing of fluids is generally performed by acoustic streaming. The driving force of acoustic streaming is also a difference in acoustic energy density, but its origin is viscous absorption in the fluid or at an interface. Acoustic cavitation is a non-linear phenomenon associated with a bubble collapse or oscillation and is used in applications such as ultrasonic cleaning and cell-poration. Acoustic cavitation occurs at frequencies lower than 1 MHz and at high pressure amplitudes and will not be considered further here.

Acoustic manipulation of particles was historically first shown in air, for the so called 'Kundt's tube' in 1874.[27] Lord Rayleigh provided extensive mathematical treatment to effects in an acoustic field,[28] giving name to effects such as Rayleigh streaming. After a lapse of many years, the scientific community was again alerted in 1971 to the acoustic forces acting on particles in a standing wave by the article published in *Nature:* 'Flow of red blood cells stopped by ultrasound'.[29] Since then, much effort has been put into exploiting acoustic forces, mainly in the field of biomedical analysis. Also, small animals such as fish, ants and ladybirds have been acoustically trapped in a quite spectacular experiment.[30]

The concept of radiation force or momentum flux may seem abstract. Some applications from other fields can serve as an illustration. A radiometer measures the acoustic power of hydrophones by measuring the deflection of a suspended sphere upon exposure to the radiated acoustic field due to acoustic radiation force. The propulsion of space crafts by solar sails exploits radiation forces, however generated by light waves rather than sound waves. A review of the recent devices in the field of acoustic manipulation of particles and cells is found in *Appendix B*.

2.1.1 A strong, gentle and long-range method for labelless or labeled particle manipulation

The acoustic radiation forces in a fluid are long-range, since the acoustic wave is present throughout the cavity. Particles anywhere in the acoustic field will experience the radiation force. Hence, pre-focusing is often not necessary.

Furthermore, the acoustic radiation forces are strong. For a typical cell density of 1050-1150 kg/m^3 and a compressibility relative water of 0.76, the acoustic radiation forces are in the range of 100 times larger than the buoyancy-corrected gravitational force at 0.5 MHz driving frequency.[31]

In addition, the acoustic forces are considered to be gentle. Based on the theoretical expression, it can be argued that in a pressure node of a standing wave a trapped particle will experience very little mechanical stress (see 2.3.3). Several studies have shown that short-term exposure to ultrasound does not have any detrimental effects on the cell viability by for instance tryphan blue-staining of hamster ovary cells.[32] Also in long-term exposure of ultrasound (12 hours) of neural cells no viability loss was found.[33] In another study the reculturing of adherent cells (from fetal monkey kidney) after 75 minutes ultrasound exposure indicated no viability losses.[34]

The MIT-platform has been evaluated for viability in *Paper 2* by growth of yeast cells during 6 hrs of trapping, and by acridine orange-staining of living RNA and DNA in neural stem cell after 15 min exposure to ultrasound.[35] Cell-viability is an issue in further testing on viable cells or for application in transplantation.

2.2 The acoustic radiation force on a particle in a fluid

2.2.1 Acoustic radiation force in a standing wave

When acoustic waves propagate in liquids, the fast oscillations may generate a non-oscillating force on particles suspended in the liquid or on an interface between liquids. This force is known as the acoustic radiation force. The force originates from the non-linearity of the propagating wave. For non-linear effects to appear, the sound wave is required to have high amplitude velocity relative the speed of sound in a fluid, *i.e.* a high Mach number ($>10^{-5}$).[36] As a result of the non-linearity, the wave is distorted as it propagates and the time-averages are non-zero. By serial expansion (according to perturbation theory) the first non-zero term will be the second-order term which accounts for both the acoustic radiation force and the acoustic streaming.[36] The acoustic radiation force on a particle in a fluid is expressed in terms of difference in radiation pressure on either side of the particle. The

radiation pressure, P, as derived from the Navier Stoke's equation can be expressed[37]

$$P = \langle p \rangle n + \rho_0 \langle v(v \cdot n) \rangle \quad (1)$$

where p is the pressure amplitude, v the velocity amplitude, n the normal vector direction and ρ_0 the density of the fluid.

The physical description of the radiation force is a superposition of the incoming wave and a scattered wave, in addition to the effect of the non-rigid particle oscillating with a different speed compared to the surrounding medium thereby radiating a wave. The derivation of the expression is performed by integrating the radiation pressure, P, or the time-average momentum flux, π, over a surface, S, enclosing the particle[38]

$$F_x = -\oint \langle \Pi \rangle dS = \oint P_x dS \quad (2)$$

It turns out that for a µm-sized particle in a MHz field the radiation pressure from a travelling wave is negligible in comparison with that of a standing wave. Therefore the systems employed for particle manipulation generally are built to create standing waves.

For a standing wave, the incident wave enters from two directions and the material-dependant parameters defining the momentum transfer are the same at the opposite surfaces. The amplitude of the pressure field, however, varies somewhat at the two interfaces, as illustrated in *Figure 2-1*. Therefore, the force will be highest where the signal amplitude is largest,[39] resulting in a net force pointing either towards or away from a pressure node.

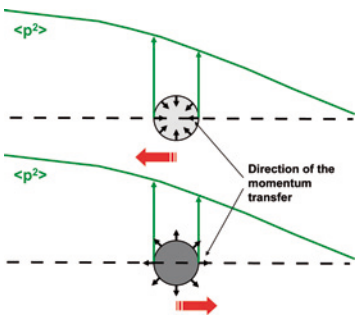

Figure 2-1. Illustration of the direction of the acoustic radiation force for a stiff and heavy (dark grey) and a flexible and light (bright grey) particle in an acoustic standing wave. The direction of radiation force is normal to the particles surface, but the magnitude of the force varies between the two sides of the particle along the axis of the wave propagation due to different magnitude of the time-averaged pressure amplitude. Hence, the net force results in a motion (large arrow) for the flexible particle towards the pressure anti-node and for the rigid particle towards the pressure node.

For a stiff and heavy particle, the radiation force is directed inwards from the particle surface and the particle is pushed to the pressure node. For a flexible and light particle in water, the force across the interface is directed outwards. Hence, the lipid will be pulled to the pressure anti-node.

Hager[39] explained that a flexible and light particle positioned in a velocity anti-node oscillate with a higher amplitude than the surrounding medium and will, at the maximal amplitude, be surrounded by fluid that has a different equilibrium position and a lower amplitude. As a result, the particle will not be fully pushed back to its origin but will, over a cycle, drift away from the velocity anti-node. The stiff and heavy particles, on the other hand, have smaller displacement than the neighboring fluid and will be pushed back by the higher oscillation of the surrounding medium and therefore stay at the velocity anti-node.

The acoustic radiation force is the spatial gradient of the acoustic radiation potential, U. Hence, for the radiation force in the x-direction, F_x, at a given point is

$$F_x = -\frac{\partial}{\partial x}\langle U(x, y, z)\rangle \tag{3}$$

where a positive value is directed towards the potential minimum. The expression of acoustic potential derived by Gorkov[40] for an arbitrary acoustic field, can be expressed as[41]

$$\langle U\rangle = \frac{4\pi r^3}{3}\left(f_1\langle E_{pot}\rangle - f_2\frac{3}{2}\langle E_{kin}\rangle\right) \tag{4}$$

where the r is the particle radius, E_{pot} is the time-averaged potential energy, E_{kin} is the time-averaged kinetic energy and the material contrast factors f_1 and f_2 are

$$f_1 = 1 - \frac{\rho_0 c_0^2}{\rho c^2} = 1 - \frac{\beta}{\beta_0}, f_2 = \frac{2(\rho - \rho_0)}{2\rho + \rho_0} \tag{5}$$

where ρ is the density in the absence of sound, c is the sound velocity and β is the compressibility which equals $1/\rho c^2$. The index *0* refers to the medium while no index is used for the particle. The time-averaged potential and kinetic energy densities are

$$\left\langle E_{pot}\right\rangle = \frac{\beta_0\left\langle p^2\right\rangle}{2}, \left\langle E_{kin}\right\rangle = \frac{\rho_0\left\langle v^2\right\rangle}{2} \tag{6}$$

for a pressure amplitude due to the sound, p, and a velocity amplitude due to the sound, v.

As can be seen, the r^3-dependence enables size-dependent manipulation and the material contrast factors f_1 and f_2 enable material dependent manipulation. The expression for the acoustic radiation force in a standing wave is given in *Appendix C*, in addition to force estimation.

In the derivation, spherical particles are assumed and the expression is valid under the requirement that particles are small in relation to the wavelength, which means that the scattered wave is transmitted in all directions.[39] In addition, the density of the fluid and the particle need to be in the same order of magnitude and the particle is assumed to be much larger than the displacement amplitude. The equation holds for arbitrary fields, with the exception of a field closely similar to that of a travelling wave. The viscosity is often neglected, *i.e.* the liquid is 'inviscid'. However, the fluid viscosity can be taken into account as a factor multiplied by f_1.[42] If the particle is cylindrical, a reorientation occurs which is faster than the acoustic displacement and strives to align the cylinder in the nodal plane.[43] Many particles of interest are not uniform throughout their whole volume. Many cells can be described as having a cell-membrane with mainly a water-like interior. In this case, the acoustic properties of the shell are different than of the cell interior. As acoustic radiation force is based on the scattering of the incident field on the surface, it is expected that the theory applies well to these kinds of particles.

2.2.2 Particle material

Acoustic sorting can be used to separate particles and the fluid medium by shifting the particles into a separate flow outlet, for instance for purifying the fluid or concentrating the particles. Additionally, separation of one type of particle from another type can be performed by exploiting the different strength of the acoustic force on the different types of particles. Typically, the flow is adjusted such that the particles have moved different distance towards the potential minima during a certain time, and are therefore collected at different outlets, such as for FFF.

The material dependence of the acoustic force in the axial direction is described by the acoustic contrast factor, Φ,

$$\Phi = f_1 + \frac{3}{2} f_2 = \frac{5\rho - 2\rho_0}{2\rho + \rho_0} - \frac{\beta}{\beta_0} \tag{7}$$

which is proportional to the force in the axial direction. In *Figure 2-2,* Φ is plotted together with f_1 and f_2 for some commonly studied particles; such as polystyrene, red blood cell and lipid.

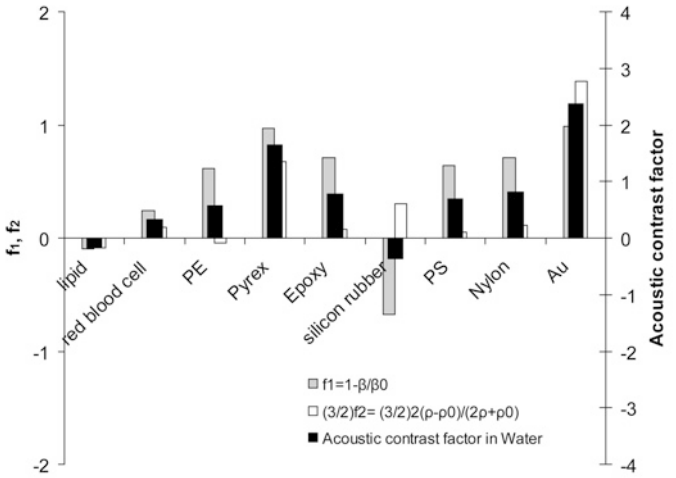

Figure 2-2. The acoustic contrast factor, Φ, and the f_1-and f_2-parameter for some different particle materials. A positive acoustic contrast factor particle moves to the pressure node, while a negative acoustic contrast particle moves to the pressure anti-node. The depth of the acoustic potential well is proportional to the f_2-factor for positive-Φ particles and proportional to the f_1-factor for negative-Φ particles. The speed of sound for a red blood cell is estimated from a compressibility relative water of 0.76.[31] (While the Φ-factor is not so intuitive it can be observed that for most cases the compressibility-dependent f_1 gives a good indication of the direction of the radiation force and an estimation of the relative magnitude.)

In the case of acoustic trapping, it is more adequate to look at the f_1 and f_2 factors separately. For an ideal standing wave, all energy is kinetic in the pressure node, and potential in the pressure anti-node. Hence, the potential well for a positive-Φ particle is proportional to f_2-factor, while it is proportional to the f_1-factor for a negative-Φ particle.

For silicon rubber, the negative f_1 value enables trapping at the pressure anti-node, while the *positive* f_2 indicates trapping at the pressure node as well. When using polystyrene particles in modeling experiments for cells, it can be noted that the sorting (axial direction) is overestimated while the trapping (lateral direction) is underestimated.

The ratio of the acoustic potential in lateral direction relative in axial direction is sometimes discussed. This is evaluated in *Figure 2-3* for an ideal standing wave and the minimal lateral potential (in the pressure node or the anti-pressure node), *i.e.* the lowest value of $E_k/\left|E_k-E_p\right|$ and $E_p/\left|E_k-E_p\right|$. For cells, this ratio is in the range of 30 % while a higher value is obtained

for lipids and glass beads (Pyrex). The lipid is therefore especially suited for trapping in the lateral direction.

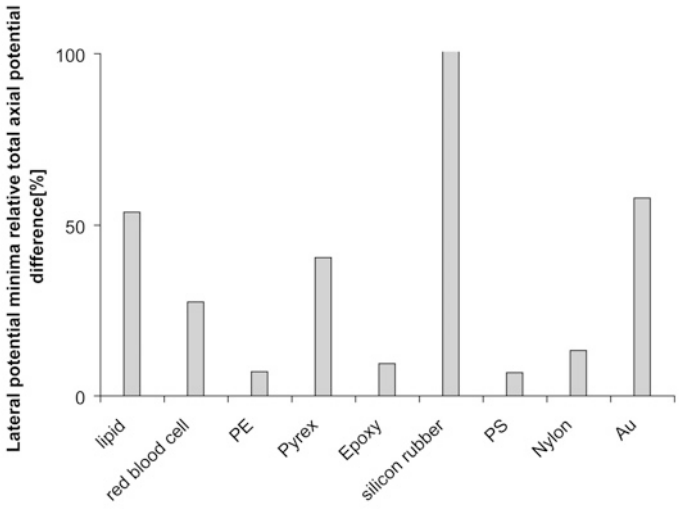

Figure 2-3. Lateral potential depth (for the lowest value at the pressure node or the anti-node) relative the axial potential, for several particle materials at pressure amplitude of 4.5 MPa and velocity amplitude of 3 m/s. An ideal standing wave is assumed and hence all energy is potential at the pressure nod and kinetic at the pressure anti-node.

2.3 Trapping in the lateral direction

The lateral acoustic forces are interesting for trapping in continuous flow. In literature, large differences exist for the ratio of lateral relative axial strength. In an article by Woodside and Piret, the lateral force was measured to be 100 times weaker than the axial force[44] as obtained by observing the speed at which the particles move to the pressure node. It is also reported that the lateral forces can be comparable to the axial forces.[45] For a Gaussian beam profile, calculations of acoustic potential show the lateral potential relative the axial potential can be in the same range.[41] Apart from differences related to the particle material parameters, the appearance of the acoustic field has impact on the strength of the radiation forces in lateral direction.

2.3.1.1 Lateral gradients from the transducer: Near field, divergence, side-lobes and clamped edges

The acoustic field of a MIT is simulated in *Figure 2-4*. It displays near field effects in the region closest to the transducer, as seen in *Figure 2-4A* and

Figure 2-4C, as opposed to the smooth decay of the pressure amplitude observed for the far field. The near field is an interference effect and can be described as originating from a line of point sources. The Near-Field Length (NFL) is defined at the last minima of oscillations on-axis, see *Figure 2-4B*,

$$NFL = \frac{a^2}{4\lambda} \tag{8}$$

where a is the diameter of the aperture and λ is the wavelength. Since the aperture is small for the MIT, the NFL is relatively long. The near field for a quadratic transducer is different than for a circular transducer since the pressure amplitude never reaches zero. No near field occurs for an aperture diameter equal to $\lambda/2$, and for still lower frequencies the radiation of the piston approaches that of a point source.[46]

Divergence of the beam and occurrence of side-lobes, can also be observed in *Figure 2-4A*. Divergence occurs of the main lobe in the far field and affects the distribution of energy in the radiated beam. Generally, a higher frequency relative the aperture generates a more directional field. Since this effect occurs in the far field, constructive interference by reflection is required to contribute to the acoustic potential landscape. Though, the beam divergence decreases the energy remaining in the main lobe.

Side-lobes are generally observed in the far-field unless the aperture, *2a*, relative the wavelength is sufficiently small (ka<3.83, k=2π/λ).[46] For the MIT plotted in *Figure 2-4, ka* equals 40 (aperture of almost 7 wavelengths).

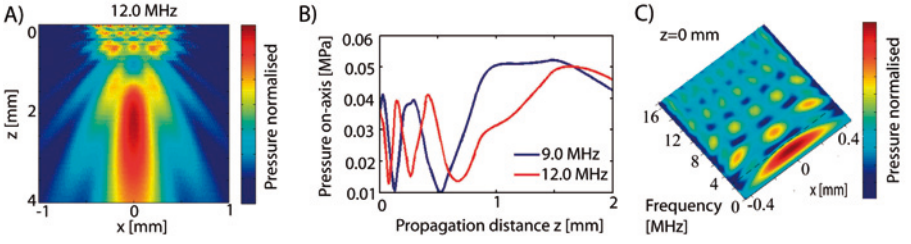

Figure 2-4. Simulation by DREAM Toolbox[47] of the acoustic pressure for a quadratic transducer A) propagating from the transducer surface for 12 MHz and B) on-axis values for three drive frequencies and C) at the transducer surface as a function of driving frequency.

2.3.1.2 Lateral gradients within the acoustic trap

Lateral variations of the acoustic field within the trap can be caused by the acoustic near field. Observed lateral forces can also have other origins, such as cavity modes and lateral modes in the transducer that are transmitted to the fluid.

The acoustic potential, *U*, of the MIT can be simulated in FEM, *Figure 2-5* (in 2D for simplicity). The transducer is represented by a line of constant velocity in *Figure 2-5A*, thereby excluding the different modes in the transducer and only accounting for near field effects. If modeling the transducer as a piezoelectric volume excited by an electrode potential, *Figure 2-5B*, both the acoustic near field and the transducer modes has been taken into account. In both cases, strong variations in the acoustic potential can be observed. Frequencies can also be found for which the lateral variations within the trap are less pronounced.

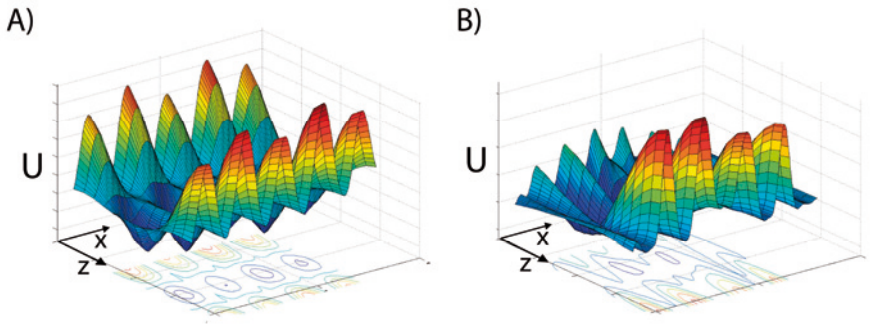

Figure 2-5. 2D simulations of the acoustic potential field, *U*, for polystyrene particles for the MIT-platform and the transducer simulated as A) a line of constant velocity or B) as a volume element exited by electrical potential. The z-direction is the wave propagation direction and the x-direction is along one of the widths of the transducer.

Analysis of the acoustic field has been performed by Lilliehorn et al.[48] in terms of the trapping pattern, by Angular Spectrum Approach (ASA) simulation for one reflection and light diffraction tomography without the reflector.

As opposed to a perfect standing wave, lateral gradients occur at several points throughout the trap and not only at the edges of the acoustic zone. In some applications this is beneficial while undesirable in others. For instance, forces acting on several points of a cluster may enable more stable trapping.

If the transducer surface does not move as a baffle but the edges are clamped, such as may occur for the MIT, reduced amplitude towards the transducer edges is expected, which decreases the lateral acoustic forces.

The near field is inherently stationary, displaying positions of maxima and minima pressure oscillations in space. Since the spatial period of the on-axis pressure amplitude increases with propagation distance, no channel height enables ideal constructive interference. The potential well is therefore not as deep as for an ideal standing wave. However, it can be expected that the cavity is less sensitive to frequency mismatching.

2.3.2 Spurious channel modes

Undesired acoustic modes can appear in the channel and around the outlets. These modes can degrade the performance by generating irregular acoustic patterns especially if operated at low flow, as explained by modeling the total channel structure[49, 50] and for the structure and a wedge transducer source[51].

The spurious modes can arise due to the divergence of the acoustic beam, the excitation of the whole channel structure or by the wave-guiding property of the fluid. The latter means that when the fluid layer is excited from the channel side-wall at a frequency higher than the half-wavelength of the channel, a component of the field will propagate along the channel and can therefore generate lateral cavity modes.

Spurious modes are not commonly observed for the MIT or the IDT platforms in this thesis. The MIT does not employ a coupling layer but acts on the fluid directly and is small in comparison with the dimensions of the channel. Hence, most of the acoustic energy is localized to the fluid volume above the transducer. The IDT have large aperture, in the range of 1 cm, relative the wavelength and hence the divergence of the wave is small. The occurrence of spurious modes in this case, also depends on how the wave is coupled into the fluid.

2.3.3 Estimation of mechanical stresses on a trapped particle

For most particles or cells the acoustic trapping occurs in a pressure node, *i.e.* where the velocity amplitude is maximum. For estimating stresses on a cell, the cell-membrane is assumed move with the particle velocity in the sound field.[36] The stresses that arise across the surface of the oscillating particle are small as long as the particle diameter is small relative to the difference in displacement on either side of the particle. With a maximum displacement amplitude in the range of nm (*see Appendix C*) and a Q-factor of 30, the displacement difference across the surface is less than a few percent per micrometer. Hence, low mechanical stresses are expected during trapping. For lipids trapped at the pressure-anti-nod, with a stress amplitude in the range of MPa, the relative change of the radius will be in the range of 10 % ($\Delta V = -\beta V \Delta P$).

2.4 The acoustic radiation force on a density interface

The direction and strength of the acoustic radiation force on a fluid interface is of interest for the manipulation of fluids, such as employed in *Paper 4-5*. The acoustic radiation forces at a density interface was demonstrated in 1939,[52] for the set-up in *Figure 2-6*. The interface was shown to move in

response to the radiation force and the direction of the movement was independent of the direction of the wave propagation but depended on the material properties of the fluid.

An expression including both the density and the speed of sound of the fluids on either side of an interface was derived by Rozenberg.[38] This expression also yields the observed results of different direction of the radiation pressure and similar magnitude for the two cases in *Figure 2-6*. Additionally, it can be used for other boundary conditions, such as constant pressure amplitude or constant velocity amplitude. It also includes different direction of the interface surface relative the wave propagation direction. The resulting expression can depend on either or both the density and the speed of sound for the fluids. In analogy with these expressions, the radiation force on a density interface perpendicular to the wave propagation was derived in *Paper 4*.

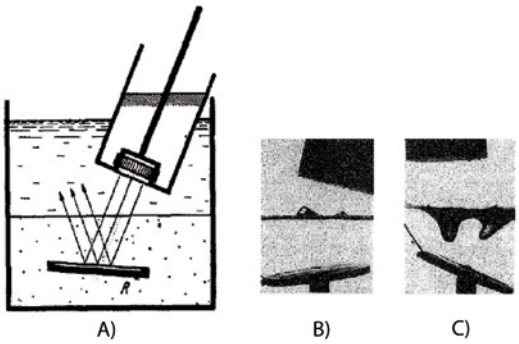

Figure 2-6. A) Illustration of a set-up with a transducer and a reflector (*R*) that is used to demonstrate the radiation force on a surface, and the independence of the fluid motion on the wave propagation direction. Experimental results for B) carbon tetrachloride (CCl_4) over water and C) water over aniline ($C_6H_5NH_2$). Both fluids have higher density than water. By assuming constant intensity, *I*, on either side of the interface, the equation for radiation pressure, *P*, $P=I/c$ was used to explain the effect. (*With kind permission from Springer Science + Business media: [52])*

2.5 Acoustic streaming limiting small particle manipulation

2.5.1 Acoustic streaming

Acoustic streaming is a phenomenon that may occur in addition to the acoustic radiation forces when radiating an acoustic wave into a fluid. In particle trapping applications, the acoustic streaming is generally undesirable since it can drag particles out from the trap which are then lost. In particle sorting, it may also disturb the effect.

Whereas the acoustic radiation force acts on an interface, acoustic streaming is a volume effect. Acoustic streaming can occur close to a surface boundary or in the free field. The mechanism of acoustic streaming is viscous losses, and the effect is therefore inherently associated with temperature increases in the fluid.

Acoustic streaming can be described in terms of radiation pressure, and its driving force is a gradient in the acoustic energy density that arises due to acoustic absorption in the fluid or due to viscous losses at a boundary. Hager emphasized that the origin of acoustic streaming is the rotational motion of the molecules in the fluid upon exposure to the acoustic field.[39]

In addition to a driving force, the fluid must have the ability, i.e. space, to move.[53] To prevent streaming, a thin membrane can be inserted in the chamber,[53] or alternatively a gel can be used in part of the chamber[54]. Streaming occurs in standing waves as well as in traveling waves.

2.5.2 Small particle manipulation

If the acoustic streaming is present, it dominates over the radiation forces for small particles. The acoustic streaming is proportional to r by Stokes drag force (see *Appendix A*) while the radiation force is proportional to r^3. Hence, the relative ratio is proportional to $1/r^2$ and therefore increases rapidly for small particles.[53]

If the acoustic streaming does not occur, the ability to handle small particles is expected to be extended. Ignoring the acoustic streaming, the manipulation of a 1 µm particle at 10 MHz translates a 0.6 µm particle at 40 MHz. A uniform acoustic field is expected to be advantageous for avoiding acoustic streaming. It may be speculated that if no vertical walls are present in the acoustic zone, the Rayleigh streaming is not generated. The MIT platform for instance have few vertical walls in the acoustic zone, *Figure 2-7A,* and streaming is not commonly observed. As opposed to a set-up with many vertical walls in the acoustic zone, *Figure 2-7B,* which has been demonstrated to generate mixing by acoustic streaming.[55]

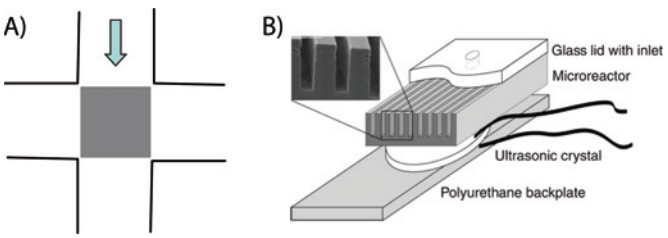

Figure 2-7. A) Top view of a fluidic channel crossing with a MIT in the bottom channel wall (grey). B) Design where many vertical walls are present in the acoustic zone and streaming is exploited. (*With kind permission from Springer Science + Business media*:[55].)

The manipulation of polystyrene particles smaller than 1 μm diameter in continuous flow in microchannels is not commonly reported in literature,[35, 50, 56, 57] though has been manipulated in larger scale-systems.[58] In *Paper 8* we demonstrate the ability to handle 0.5 μm polystyrene beads. Biological particles such as bacteria are as small as 0.5 μm diameter and viruses are in the range of 0.1-0.3 μm diameter. Proteins are less than 0.1 μm.

In some cases, the acoustic streaming add to the effect of the radiation force, such as for a rigid particle in a standing wave where the streaming velocity points in the direction of the pressure node.[39]

If the acoustic streaming does not occur, the ability to handle small particles will instead probably be related to viscous effects. Modifications of the general equations for radiation pressure have been performed, to account for viscous and thermal effects.[59-62] For standing waves and small particles relative the viscous boundary layer, the theory predicts that the viscous boundary layer can alter the radiation force significantly in magnitude and direction. It is explained as a sharp variation of the momentum flux in the boundary layer which carries away part of the momentum flux brought by the sound wave.[62] The author evaluated the expression by Danilov[62] (which does not include compressibility) at 10 MHz for nylon particles and cells, and found that particles in the range of 0.3 μm or smaller are more strongly affected by the acoustic radiation force than what is predicted by the general theory. The gathering of as small as 0.3 μm polystyrene particles has been demonstrated in practice (0.5 MHz, 50Vpp) and a shell layer suggested to accounting for the observed radiation force in the same range for 0.5 μm particles as for 2 μm particles.[63]

3 Transducer and microchannel

3.1 Acoustic transducers

An electromechanical device for generating a pressure wave is called a 'transducer' or an 'actuator', since it translates an electrical signal into a mechanical response and can be used to act on, for instance, a fluid. Traditional applications for acoustic transducers are medical diagnostics hydrophones and marine sonars. Similar to these transducers, the MIT employ Bulk Acoustic Waves (BAW). Surface acoustic wave (SAW) transducers are used in the IDT-platform. SAWs are found in actuator applications such as SAW-motors and droplet manipulation devices. More traditional applications for SAWs are as filters in mobile phones and as SAW sensors. The transducer principle employed is called piezoelectric and the word *piezein* in Greek means *to press*.

3.2 Piezoelectric materials

A commonly used piezoelectric material is the PZT ($PbZr_{(1-x)}Ti_xO_3$). It has an exceptionally high dielectric constant (d in the range of 300 pC/N). This means that an applied voltage generates a large displacement. Though, practical strains of a polycrystalline PZT are still only on the order of ‰ for static operation.

The origin of the large electromechanical response in PZT is its crystal structure and the many polarization directions (14) available for the material composition usually used. A ceramic material, such as PZT, is polycrystalline and has several grains (uniform crystal orientation), which in turn comprise several domains with different polarization orientation. In PZT the large number of polarization directions enable an overall high degree of polarization. The strain and the electric displacement occur by re-polarization of the material hence motion of the domains walls. The domain wall motion is very fast; and the material can be used in GHz frequency.

All piezoelectric materials are ferroelectric and are therefore used after polarization, where the spontaneous polarization direction is aligned with the electric field. The motion of the domain wall is associated with losses (see

Appendix D) and piezoelectrically hard materials are used in resonant drive and if temperature needs to be minimized such as in some biological applications.

Lithium tantalite ($LiTaO_3$) and lithium niobate ($LiNbO_3$) used in the SAW devices in this thesis are single crystalline material. The two materials have a different crystal structure than PZT and only two possible polar directions exist (oppositely directed). As a consequence, only limited piezoelectric activity can be induced in ceramics and hence the material is used as a single crystal. Relative the PZT, the electromechanical coupling is lower while the losses are also lower, see *Appendix D*.

3.2.1 Transducer processing

PZT can be deposited by thick-film processing, by thin-film processing or by sol-gel. The MITs in *Paper 1* are in-house thick-film processed multilayer structures (EDO EC-76 and EC-69). A multilayer structure is used and the voltage required to drive the actuator is reduced relative a single layer structure. In thick-film processing, a slurry is prepared of solvent, polymer binding and PZT-powder. The mixture is cast and structured in 'green state' (rubbery state before sintering). The electrodes are deposited by screen-printing as intermediate layers. In the subsequent step, the laminated multilayer structures are sintered at 1200 °C during which the polymer binding is removed and the material shrinks approximately 20%.

The hard PZT in *Paper 1* was considerably more difficult to polarize than the soft PZT. For this reason and to decrease the manufacturing time, the thick-film processing was replaced by dicing a commercial single layer plate. The higher voltage requirement for single layers is usually not a large concern in the biomedical applications addressed.The MITs in *Paper 2-5* are single layer disks (Ferroperm Pz26).

Single crystalline piezoelectrics such as $LiNbO_3$ and $LiTaO_3$ are grown from a melt and the material cost is therefore higher.

3.3 Bulk Acoustic Wave (BAW) and Surface Acoustic Wave (SAW)

Different modes can be excited in a piezoelectric plate. For bulk acoustic waves (BAW), the entire volume of the material is deformed while for the surface acoustic waves (SAW) the deformation is located to the surface of the material. To actuate a BAW, the electrodes are deposited on either side of the piezoelectric volume. A SAW can be actuated by Inter Digital Transducer (IDT) which is a structure of metal strips on the surface of the piezoelectric substrate.

The BAWs in guided plate geometry are known as Lamb modes, and are either symmetric or antisymmetric. The intensity of the Lamb modes excited in a structure depends on its diameter-to-thickness ratio.

Dispersion curves can be calculated to display the occurrences of the modes as a function of frequency. The thickness-mode appears at a frequency, f_0, which is related to the thickness, d, and the wave velocity, v_{stiff}, by $f_0 = v_{stiff}/(2d)$, where the stiffened wave-velocity occurs since the internal generated electrical field is in the same direction as the wave propagation. This resonance is observed as a parallel resonance in the electrical spectra. At this resonance, the electrical displacement generated from the strain is equal and opposite to the electrical displacement generated from the internal electric field and hence the total electrical displacement is zero. The largest amplitude of the piezoelectric volume is obtained where the applied voltage is in phase with the induced current, which occurs at the series resonance frequency.

For SAWs, 90 % of the energy is confined within one wavelength of the surface. The frequency of the SAW is determined by the distance between the electrodes, $f_0 = v/\lambda$, where the wavelength is determined by the electrode period. The SAW motion is elliptical since it is a combination of a longitudinal wave and a shear wave.

3.4 The microfluidic channel material

In academia, the most common microfluidic channel materials are poly(dimetyl siloxane) (PDMS), glass and silicon. In the industry, where mass-fabrication is employed, thermoplastics such as polycarbonate (PC), poly(metyl mathacrylate) PMMA and cycloolefin-copolymers (COC) are often processed by injection molding.

3.4.1 PDMS channel

PDMS is a silicon rubber and offers fast prototyping and easy bonding to itself or other Si-based surfaces after surface activation by for instance oxygen plasma. Usually, a structured PDMS layer is bonded to a glass slide. Other properties of PDMS are transparency in UV and visual wavelengths and mechanical flexibility. The high gas-permeability of PDMS makes it suitable for cell culturing applications. However, the adsorption to the surfaces and the release of monomers can be a limiting factor in some applications.

Surface treatments are often necessary; oxidation minimizes the adsorption of hydrophobic analytes and Heparine (polysaccharide) coating minimizes the adsorption of biological samples. However, the surface modification can degrade over time which affects long-term usage and storage.

PDMS is manufactured by soft lithography, where a mold is cast with PDMS to cure in oven at 70 °C.

For application in acoustic manipulation, the high acoustic absorption in polymer materials generally makes them less suitable channel materials. In a few cases, polymer channels have been employed such as PDMS *in Paper 6,* and similar[64] or by mounting a transducer in air pockets on either side of a PDMS channel[65]. In other cases, a polymer is used as the channel spacer on a unstructured reflector layer, such as PDMS[34] and SU-8[66]. PDMS has also been added in part of the spacer layer to reduce cavity modes.[67]

3.4.2 Glass channel

Glass, such as borosilicate, is generally a more expensive material than polymers. However, it is hydrophilic, inert and transparent in the visual range (but not in UV). Surface modification methods of glass are well known since it is conventionally used in capillary electrophoresis and in microarrays.

Structuring of glass can be performed by wet etching or dry-etching. The isotropic wet-etching generates quarter-spherical or tapered walls and under-etch. Two wet-etching recipes were used in this thesis for borosilicate glass, 1) a fast etch rate of 8.5 µm/min for 1:10 HF:HCl and 2) a slower etch of 1 µm/min for HF:HNO3:DI water (100:28:72, v/v) with sonication every 5 minute. The sonication was performed to remove oxides that were observed to form on the surface. The fast method generated a channel profile of tapered walls and walls with ridges, *Figure 3-1A*. For the thick mask (of metal and photoresist) used, very few pinholes were observed. Pinholes may disturb the wave, if located along its path. The slower method enabled a quarter-circular profile and smooth channel walls, as observed in *Figure 3-1B and C*, but resulted in more pin-holes for the thinner mask used and the longer etch-times.

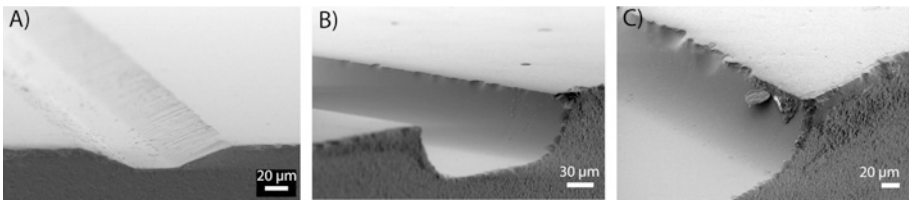

Figure 3-1. Cross-sections of wet etched borosilicate channels. A) Narrow channels etched by a fast recipe and B) wider channels etched by a slower recipe.

Dry etching of glass is considerably slower, 0.6 µm/min[68] for Deep Reaction Ion Etching (DRIE) and 0.2 µm/min[69] for Inductively Coupled Plasma Reactive Ion Etching (ICP-RIE).

Glass can be bonded by anodic bonding to a conductive material, such as silicon, provided that the surfaces are smooth (surface roughness in the range of a few nm) and if the two materials have similar thermal expansion coefficients. A bonding technique tolerant to surface roughness is adhesive bonding,[70] which was employed in *Paper 7-8*. A cross-section of the bonded channel in *Paper 8* is shown in *Figure 3-2*. The channel material is fused silica, wet etched by HF:H_2O 50:50 with a polysilicon mask at a speed of approximately 1.6 µm/min.

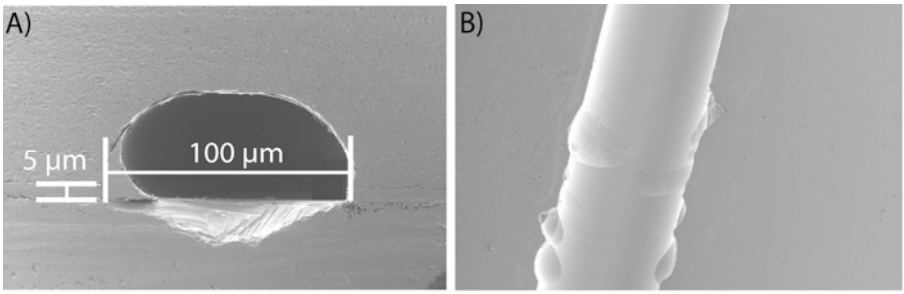

Figure 3-2. A) Cross-section of the 100 µm wide wet etched silicon dioxide channel adhesively bonded to the lithium tantalite substrate by a 5 µm thick SU8 layer. B) The surface of the etched silicon dioxide channel is very smooth but displays cup-shaped irregularities in the surface probably due to impurities in the material.

3.4.3 Channel integrated components

For the MIT platform, *Papers 1-5,* the transducers were cast in epoxy and the transducer/epoxy surface constituted the lower channel wall. Sealing to the channel structure was performed by clamping since one of the materials is soft and it allows for reopening.

Epoxies display excellent adhesion to most materials and are a thermosetting polymer that cures by mixing with a catalyzing agent, by heat, UV-light or moisture. Epoxies exist with a wide variety of properties such as chemical and heat resistance, mechanical properties and electrical insulating or electrically conducting. Channel shrinkage during curing is a factor to consider as well as low auto-fluorescence and low water absorption.

To improve the scratch resistance, a surface coating of the epoxy-PZT layer by Parylene was used in *Papers 4-5*. Parylene is a commonly used coating material, in biomedical applications and for PZT inkjet printheads. It offers electrical insulation, barrier for diffusion of moisture or of molecules into the fluid and biocompatibility. A thin even layer of Parylene can be deposited by chemical vapor deposition (CVD) at room temperature.

4 Acoustic multilayer cavity design

4.1 Multilayer cavity design

Several parameters influence the level of acoustic pressure inside the fluidic cavity, for instance the electormechanical coupling of the piezoelectric material, the losses of the piezoelectric material, the matching of the load to the function generator, the efficiency of the coupling of the acoustic wave into the cavity and resonance quality of the fluidic channel and the channel structure which enable energy build-up inside the cavity.

4.2 Reflection coefficient

Reflection of the wave is one way to create a standing wave and is needed to contain energy in a structure. The reflection coefficient, R,[46]

$$R_I = \frac{(r_2 - r_1)^2 + x_2^2}{(r_2 + r_1)^2 + x_2^2} \tag{9}$$

where the acoustic impedance z can be expressed in a few different ways,

$$z_2 = \frac{p}{v} = \rho_0 c = r_2 + jx_2 \tag{10}$$

where r_2 is the acoustic specific resistance, x_2 is the acoustic specific reactance, p is the acoustic pressure and v is the speed of sound in the medium. The complex value is obtained for standing waves or diverging waves as opposed to progressive plane waves. In general, high reflectance is obtained at boundaries which mismatch in acoustic impedance. For a standing wave, the reflectance at the interface is degraded by the phase term x_2. Highest reflectance (pressure doubling) at the edges of a low-impedance layer is obtained at a pressure anti-node (rigid boundary).[71] For such case, the reflection coefficient from water (r of 1 MRayl) to glass (r of 15 MRayl) is $(14/16)^2$ and to PZT (r of 45 MRayl) is $(44/46)^2$.

4.3 Optimal fluid-reflector thickness (1D)

An expression for predicting resonances in a fluid-reflector structure has been derived by Hill[71] and is used in *Paper 3*. By a transfer-impedance expression the impedance at the interfaces between the layers is obtained, as a function of the parameters in the previous layers. The transducer is modeled as very high impedance. It is further stated that the fluid-reflector structure will resonate when the reactances at the reflector boundaries are equal,

$$\mathrm{Im}\{Z_{12} - Z_{21}\} = 0 \tag{11}$$

where Z_{12} is the impedance looking from the fluid layer into the reflector layer and Z_{21} is the impedance looking from the reflector layer into the fluid layer, which yields the final expression.

4.4 Equivalent circuit model with load (1D)

Modelling of the total multilayer structure including the transducer can be performed by combining transfer-impedance expression with the transducer modeled by an equivalent circuit of lumped elements.[72, 73] More general expressions was derived by Nowotny *et al.* including also anisotropic materials[74] and piezoelectric multilayer structures[75]. The model is valid near a resonance frequency, for an isolated mode and in 1D. Several parameters that are required may be estimated from electrical impedance measurements and this model has displayed good agreement with measurements for several multilayer acoustic manipulation systems which are relatively 1D.[76] The acoustic pressure amplitude in the fluid is obtained from the force at its boundary, which is calculated as a function of the impedances at either side of the boundary and a transformation ratio between electrical and mechanical quantities.

5 Summary of the work presented in the Included Papers

5.1 MIT for acoustic trapping in bead and cell assays

Acoustic trapping in the middle of the channel height enables surface independent trapping without risk of clogging. For non-adhering cells non-contact trapping is an obvious advantage since it mimics *in vivio* conditions. The size of the acoustic trap of 70*1000*1000 μm^3 enables handling of single cells as well as cell clusters. Buoyancy forces during trapping are counteracted by the radiation force in the axial direction, enabling trapping of heavier particles and at low flow velocities.

The MIT platform can be used as a single-spot trap for cell-studies in contact-less environment, *Figure 5-1A*.

The platform can also be used for a series of elements in sequential operation. Little analyte carry-over is expected since the cells or beads are moved to the subsequent trapping site, *Figure 5-1B*.

In a matrix format the trapping platform can be used for cell assays, *Figure 5-1C*. The platform can also be used to trap surface coated beads for DNA or protein analysis as an alternative platform for microarrays.[77] Each bead coating can be prepared in bulk which makes it cheap. Further, the preparation occurs under constant conditions, which is complicated in microarrays and has is significant for proteins since they are sensitive to their environment. High flexibility is obtained since the user can select the combination of beads at the time of analysis. For read-out by flow cytometry the analysis rates can be very high. The realization of the 2D MIT platform requires solving manufacturing issues mainly regarding electroding of the multiple MITs.

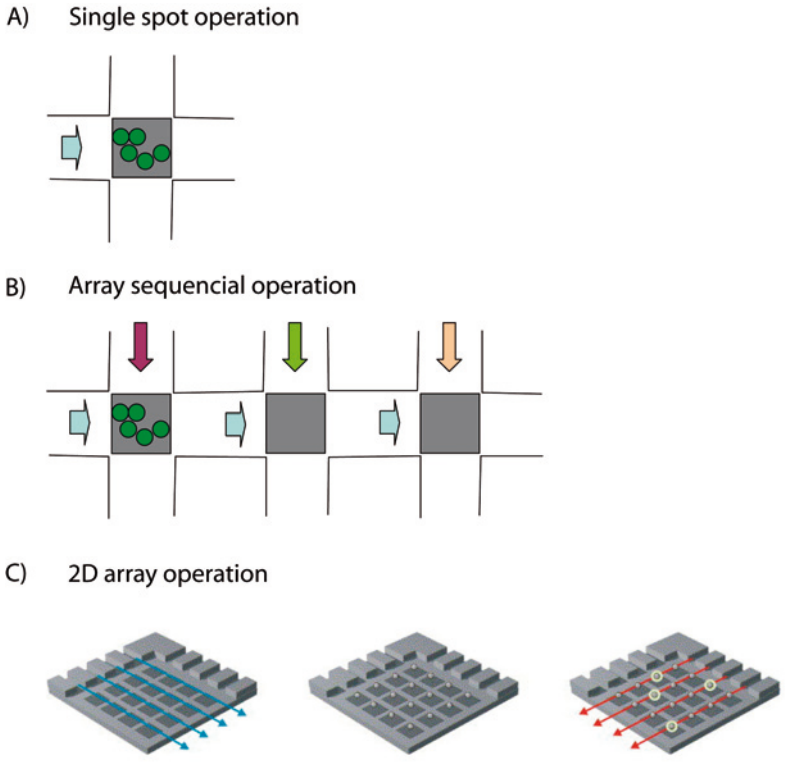

Figure 5-1. A) Single-spot operation, B) array sequential operation, C) Matrix operation with insertion of beads from one side and sample from the other side.

5.1.1 Temperature management

For cell culturing or cell assays, the duration of cell handling can be of considerable length, which accentuates the temperature increase as an important performance parameter. Temperature increase in the fluid for the MIT originates from dielectric and mechanical losses in the transducer and absorption of the radiated acoustic energy at boundaries, as expressed in *Paper 3*. Temperature requirements can be below an upper value to ensure safe handling of cells and proteins or to target a special temperature range to regulate the trap environment.[78] In literature, a dual-chamber has been used with an acoustically transparent membrane of 0.25 mm polysulofone to seal off a cooling water region closest to the large-scale transducer.[79]

For the MIT, the heat is generated closer to the fluid compared with externally positioned transducers. A Finite Element Method (FEM) simulation of the temperature distribution from a quadratic element at an elevated temperature is shown in *Figure 22C*. The large surface-to-volume ratio of the MIT is expected to be favorable for minimizing the temperature increase in

the fluid since heat is efficiently transported to the surrounding material which acts as a heat sink.

In *Paper 2-3* the temperature evaluation of the fluid was performed by measuring the temperature-dependent fluorescent response of the fluorophore Rhodamine B. Initially, a fluorescence calibration curve was generated by measuring the fluorescence intensity in the channel while heating the entire platform, *Figure 5-2B*. After observing a stable temperature during at least 2 minutes, the microscope aperture was opened and an image was recorded. Adsorption of Rhodamine to the surfaces was found to influence the result and an initial stabilization step of up to 3 hrs was introduced to allow saturation of the surfaces with Rhodamine. The accuracy of the temperature measurements calculated as the standard deviation of residuals in the calibration curve was found to be 0.62 °C.

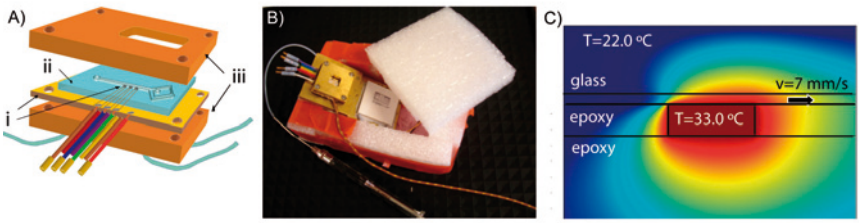

Figure 5-2. A) Illustration of the PCB with (i) integrated actuators (900*900*200 μm^3) and electrical connections, (ii) the channel and reflector structure and (iii) the clamping brass holders with through holes for fluidic interconnects and visual inspection. B) Photo of the set-up for the fluorescence calibration measurements with the thermocouple and the polymer foam container to ensure a stable thermal environment. C) Illustration of temperature profile by FEM-simulation of heat conduction and convection from a quadratic element at an elevated temperature and a microchannel with fluid flow.

5.1.2 Qualitative temperature measurements: moderate levels and fast response

In *Paper 1* the temperature and pressure output measurements were performed for in-house manufactured soft (EDO-76) and hard (EDO-69) multilayer PZT transducers. The measurements for a certain pressure level in the far field demonstrated a higher temperature increase for the soft PZT compared to the hard PZT, 5.8 ºC versus 2.2 ºC at series resonance, *Figure 5-3B*. It was observed that the temperature increase for the soft PZT was higher at series resonance frequency than at parallel resonance frequency for a given pressure output. The acoustic pressure was measured in water with a needle hydrophone at 25 wavelengths distance from transducer surface.

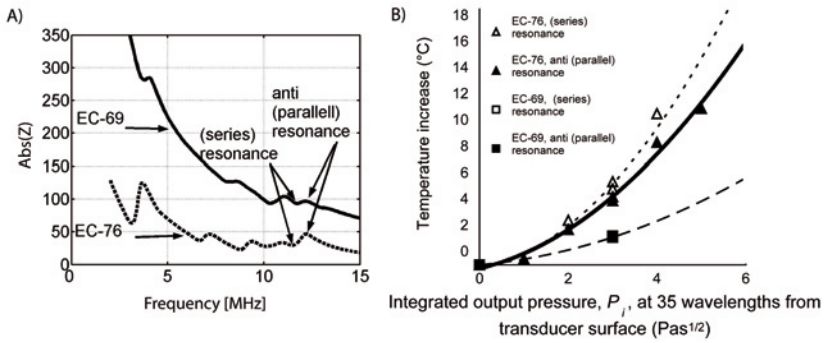

Figure 5-3. A) Electrical impedance spectra with thickness resonances marked for piezoelectric soft (EC-76) and hard (EC-69) PZT. B) Thermal measurements with Rhodamine B in the microchannel as a function of the acoustic output in the far field of the unloaded transducer. (For EC-69 the curve is predicted assuming a linear relation between temperature increase and pressure amplitude.)

For the single layer transducers in *Paper 2* and a driving voltage of 7 Vpp (at which level several single layer transducers showed good trapping of 5 µm polystyrene particles) the temperature increase was 7.2 °C yielding an absolute temperature of 30.0 °C for a certain driving frequency. In *Paper 3* at 10 Vpp operation and for a level of trapping strength of 60 au, which corresponds to a high coverage of the trapping area, the temperature at the optimal driving frequency was 32 °C, a temperature increase of 7 °C in that case.

The temperature response was found to be fast with a fall-time of 8 s and a rise-time of 11 s, *Figure 5-4*. For a temperature-compensated system, a fast response is an advantage since a stabilization of temperature is not expected to be performed faster than the time frame of the disturbance.

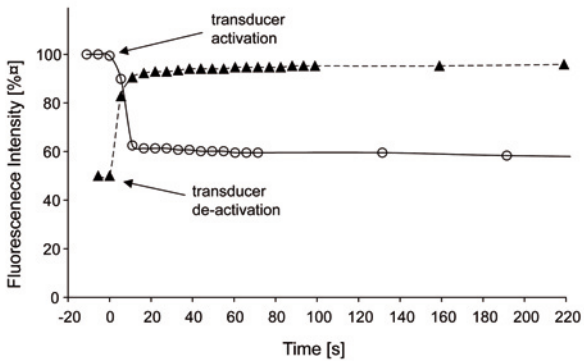

Figure 5-4. The normalised intensity response for transducer activation and deactivation, at 10.7 Vpp and a fluid flow of 0.1 mm s^{-1}. The fall time was 8 s and the rise time was 11 s between intensity levels of 90 % and 10 %.

5.1.3 High degree of linearity of the miniaturized transducers

Miniaturization of the transducer imposes uncertainties in the prediction of performance. The low width to diameter ratio causes a large deviation from the case of a plate thickness mode and spurious modes where commonly observed in the impedance data.

In *Paper 2,* the fluorescent temperature measurements were evaluated for increasing driving voltage, and the transducers displayed a high degree of linearity, *Figure 5-5A*. In *Paper 3*, the acoustic pressure in the far field also displayed a high degree of linearity, *Figure 5-5B*. The trapping strength for a cluster of particles, for the assumption of an elliptic paraboloid shape of the acoustic potential well, *Figure 5-5B,* also displayed approximate linearity.

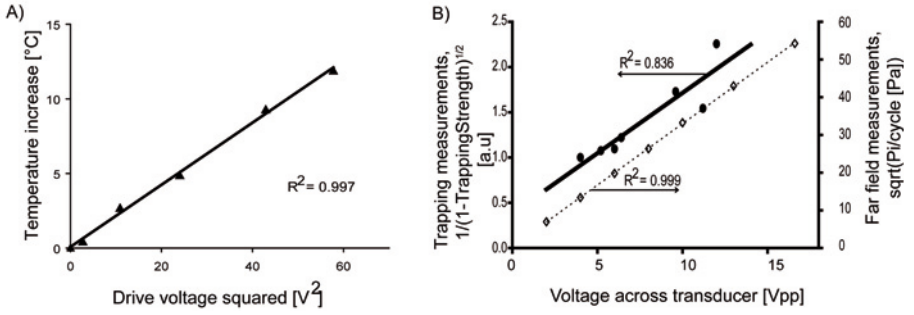

Figure 5-5. A) Temperature increase as a function of driving voltage from *Paper 2*. B) Acoustic pressure output and trapping strength as a function of driving voltage from *Paper 3*. The 1/(1- trapping strength)1/2 (●) and the square root of the acoustic pulse-pressure squared integral, Pi, (◊), per cycle in the acoustic far field.

5.1.4 Trapping strength measurement: single particle and particle cluster area

In *Paper 2*, single-particle force measurements were performed based on balancing of the acoustic radiation force in lateral direction with Stokes drag force. A particle was trapped and the flow was increased in steps of 1 µL/min until the drag force exceeded the radiation force and the particle was dragged away from the trapping site. The magnitude of the force on 10 µm polystyrene particles was 430±135 pN corresponding to balancing a hydrodynamic flow of 4.6±1.4 mm/s for a driving voltage of 7 V_{pp}. The measurements were based on six repetitive measurements. The relative large deviation of 30 % was probably related to the particle being trapped at different positions in the potential landscape. The trapping force on the 0.87 µm polystyren particles was found to be very weak while the 1.8 µm particles were easily trapped.

In *Paper 3,* the trapping strength was measured as the projected area of a trapped cluster of 5 µm polyimide particles, counter-balanced by the hydrodynamic force. Particles were trapped upon activating the transducer and, when turning on the sheath flow, the projected area of the cluster of particles still trapped against the hydrodynamic drag force was recorded. The flow velocity was 2 µL min^{-1} (0.5 mm s^{-1}). The mean intensity of the B/W images, proportional to the size of the cluster, was interpreted as trapping strength, *Figure 5-6*.

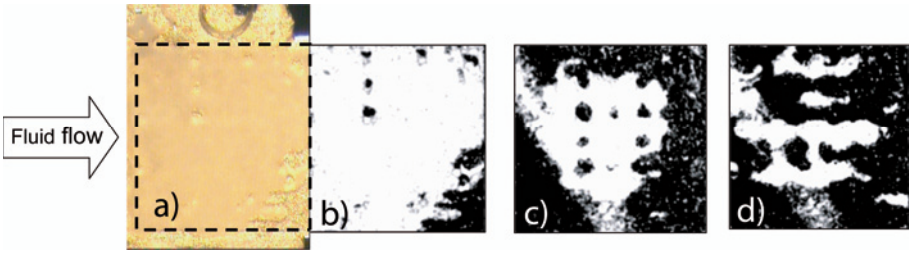

Figure 5-6. The projected area of trapped particles (diffuse/white) against the transducer surface (high reflectance/black) at 2 µl min^{-1} fluid flow. For a concentrated particle plug at 11.2 MHz (a) colour image with transducer area indicated and (b) the converted B/W image and for a diluted plug at (c) 11.2 MHz and (d) 10.6 MHz. A scratch in the reflector top surface going diagonal across the image is visible.

The trapping strength at different positions in an acoustic trap at a continuous flow, was analytically expressed in terms of the work needed to escape the trap in the direction of the flow, W_{escape},

$$W_{escape}(x_i, y_i, z_i) = \int_{x_0}^{x_{ref}} F dx = -\int_{x_0}^{x_{ref}} \frac{\partial}{\partial x} \langle U(x_i, y_i, z_i) \rangle dx = \\ = \langle U(x_i, y_i, z_i) \rangle - \langle U_{ref} \rangle \tag{12}$$

where the index i refers to a selected position in the trap and the reference potential, U_{ref}, is the potential level at which the particle is free. At the bottom of the acoustic potential well, the radiation force is zero but the particle is not free to leave the trap and W_{escape} is not zero. U_{ref} can be a zero level outside the transducer or a positive potential barrier present in the particle's path to escape.

5.1.5 Viability evaluation

In *Paper 2,* the viability of the MIT platform was evaluated to see if the gentleness that is generally reported in literature for manipulation in ultrasonic standing wave devices also holds for our platform and for the somewhat higher frequencies employed.

Viability was evaluated by observing the growth of yeast cells in the trap during 6 hours at 7 Vpp. The cells were found to be growing and viable, as shown *Figure 5-7A*. In addition, neural rat stem cells were evaluated by Acridine Orange after being trapped for 15 minutes at 7 Vpp. Staining of the cell RNA and DNA by Acridine Orange was observed which only occurs for living cells, *Figure 5-7B*.

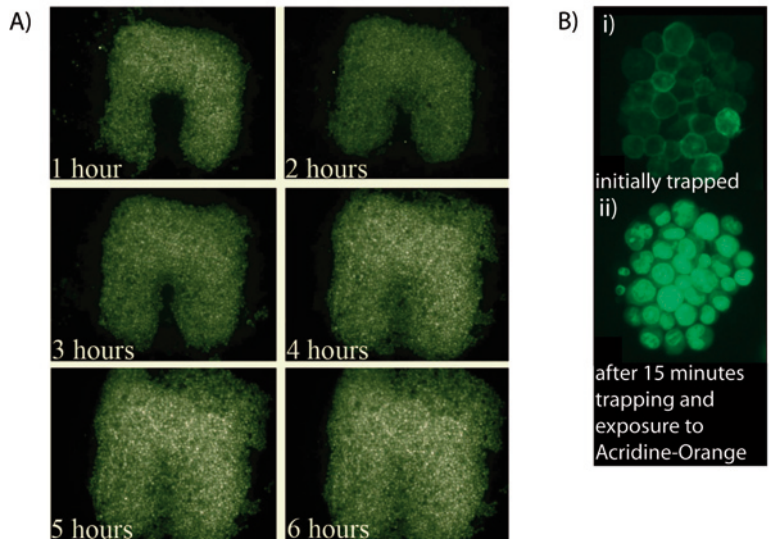

Figure 5-7. A: Growth of Yellow Fluorescent Protein expressing yeast cells, trapped in the acoustic device while being perfused with cell medium. The increase in the number of cells indicates that the cell proliferation is not affected by the acoustic radiation. B: A viability assay on a cluster of neural stem cells, modified to express Green Fluorescent Protein. In (i) the cells are shown shortly after being trapped and in (ii) after 15 minutes in the trap after which they were perfused with Acridine-Orange. The Acridine-Orange migrated into all the cells initially visible, indicating a viable cell cluster.

5.1.6 Optimal driving frequency

To evaluate the optimal driving frequency of the MIT platform the trapping strength and temperature increase was measured for a frequency interval of ± 15 % relative to the driving frequency, in *Paper 3*. The voltage from the function generator was adjusted to obtain a constant level at the transducer. In the future, a matching network can be used to optimize the coupling from

the function generator to the transducer. For the evaluated set-up, the transducer resonance frequency is lower than the channel λ/2-frequency.

Relatively low values of resonance quality factors, Q, were obtained for the transducer series resonance (28) as well as for the assembled system (33). However, this renders the cavity insensitive to frequency variations during operation that can occur due to temperature variations, *Figure 5-8B*. In literature, several standing-wave systems are operated with automatic frequency regulation to account for drift of parameter values.[80, 81]

The temperature increase was found to be proportional to the active power, P_{active}, with a peak value of 15 °C temperature increase at the series resonance for 10 Vpp, *Figure 5-8A*.

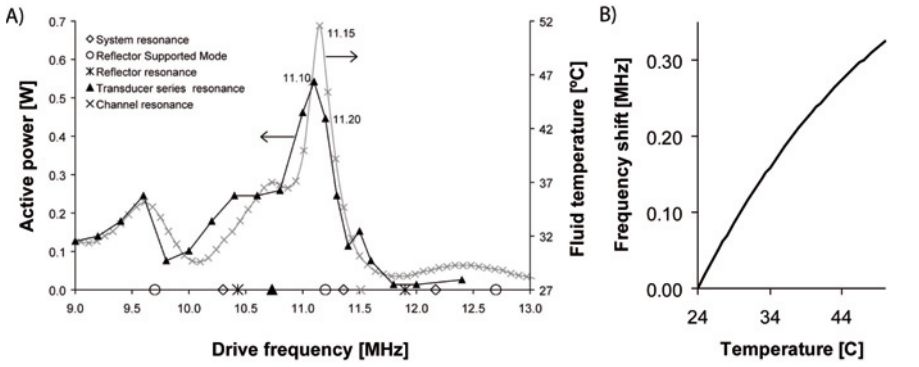

Figure 5-8. The temperature increase (-▲-) in the channel and the active power (-x-). A close to linear relation between the active power and the heat generated is observed. The frequencies indicated are the reflector supported frequencies (o), the system resonances (◊), the λ/2 resonance in the channel (x), the reflector resonances (*) and the transducer series resonance (▲). The ambient temperature was 24.8 ± 0.2 °C. B) Frequency shift for a temperature increase due to a change in sound velocity.

Upon transducer activation, the particles in the fluid were immediately displaced. Trapping was observed at every frequency, with a few exceptions, in the interval 9-11.5 MHz. The main peak in the trapping strength curve displays a double peak shape, *Figure 5-9A*. The leftmost peak (11.2 MHz) coincides with the *peak in active power* (11.15 MHz). The rightmost peak (11.4 MHz) coincides with the *calculated system resonance* (11.35 MHz).

The results are in agreement with measurements of displacement by acoustic force balance instrument where the peak displacement is found at the peak active power.[82] Also for multilayer systems it has been observed that a peak in active power corresponds to a peak in mean displacement.[83]

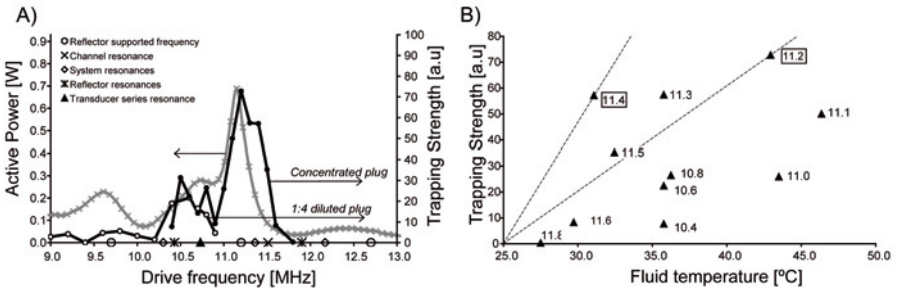

Figure 5-9. A) The active power (-x-) and the trapping strength for the concentrated plug (-●-) and for the diluted plug (-○-) of particles at fluid flow of 2 µl min^{-1}. B) The trapping strength versus the fluid temperature in the interval 10.4-11.8 MHz, indicates that the parallel resonance frequency (11.4 MHz) is more favourable than the series resonance frequency (between 11.1 and 11.2 MHz), when taking both the temperature and the trapping into account. Moving along a straight line from origo corresponds to increasing the driving voltage. A high slope indicates a more efficient driving frequency.

The trapping-to-temperature efficiency was recorded and the peak was observed to occur at the calculated system resonance in the fluid-reflector structure also coinciding with a parallel resonance, *Figure 5-9B*. The results emphasize the importance of selecting the proper driving frequency for long term handling of cells, as opposed to the more pragmatic way of selecting the frequency of the highest acoustic output.

Driving an actuator at parallel resonance is in general associated with low energy consumption, but the observed advantage in trapping-to-temperature efficiency is believed to be mainly attributed to better confinement of energy in the fluid. For a high-loss material, the parallel resonance is found to be rather close to the series resonance *i.e.* at the slope of the Re(*A*)-peak and the displacement is therefore not insignificant. Regarding efficient driving Gröschl[79, 84] reported peaks in efficiency at the series and the parallel resonance frequencies, with optimum close to the transducer parallel resonance.

5.1.7 1D Resonance modeling

A prediction of resonance peaks for the composite fluid-reflector-layer by a transfer-matrix model[71] was used for identifying 'system resonances'. These resonances indicate energy maxima in the system which is assumed to also generate high energy in the fluid layer. For our case with the speed of sound in the borosilicate glass of 5540 ms^{-1} and in the fluid of 1500 ms^{-1}, the analytical expression yields the diagram in *Figure 5-10*, for the range of layer thicknesses of interest. The system resonances are found at an intersection of the curves, found at for instance 10.30 MHz and 11.35 MHz. Moving along the straight line corresponds to increasing the frequency for the selected design.

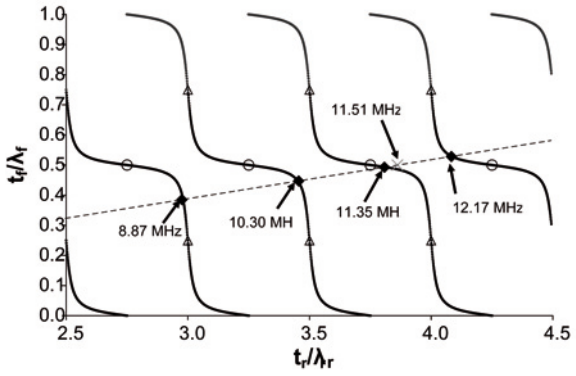

Figure 5-10. The diagram predicts system resonances where the two curves intersect for various selections of reflector and fluid layer thicknesses expressed in wavelengths.[71] System resonances (♦) are found at 8.87 MHz, 10.30 MHz, 11.35 MHz, 12.17 MHz and 13.50 MHz respectively.

Trapping was observed at all but a few frequencies in the evaluated interval. Fundamentally, trapping requires a stationary field, which is obtained for a standing wave and also without reflections for the near field.

However, for the near field reflections can increase the amplitude of the acoustic field. Highest reflectance (pressure doubling) at the edges of a low-impedance layer is obtained at a pressure anti-node (rigid boundary).[71] In *Paper* 3, such a frequency is called 'reflector-supported frequency' and corresponds to the frequency of the most significant peak in the trapping measurements at 11.2 MHz and the peak at 9.7 MHz.

In conclusion, the resonances obtained from the 1D analytical expression in addition to the reflector-supported frequencies correlate with the significant peaks observed in the impedance measurements, the temperature measurements and the trapping strength measurements. This suggests that a 1D-model can be a good first approximation of the system despite the 2D characteristics observed in the trapping pattern and the low diameter-to-thickness ratio of the transducers which generates lateral modes in the transducer.

5.2 MIT for fluidic mixing

In *Paper 4*, the Miniaturized Integrated Transducers (MIT) platform was evaluated for acoustic mixing by radiation forces on a density interface. The mixing occurs at a fluid-fluid density interface due to the acoustic radiation force. Surface effects become more pronounced in the micro scale, enabling the utilization of effects that are insignificant in the macro scale. To the best of our knowledge, the mixing by acoustic radiation forces at a density interface within a microfluidic system has not previously been described.

The lateral dimensions of the transducer (900*900 μm) enable local activation in a small area of the channel. The density interface is created between the higher-density fluid of 17 % glycerol/DI water and the lower-density fluid of DI water. Mixing is measured by the peak broadening of the fluid labelled with Rhodamine B, *Figure 5-12B*. In *Figure 5-11A*, the primary sample flow (1) contains the fluid with density different than the other flows. The evaluated total volume flow in the main channel was 2.6-85.0 μL min^{-1} (0.6-20 mm s^{-1}) corresponding to a Reynolds number of 0.08-2.5.

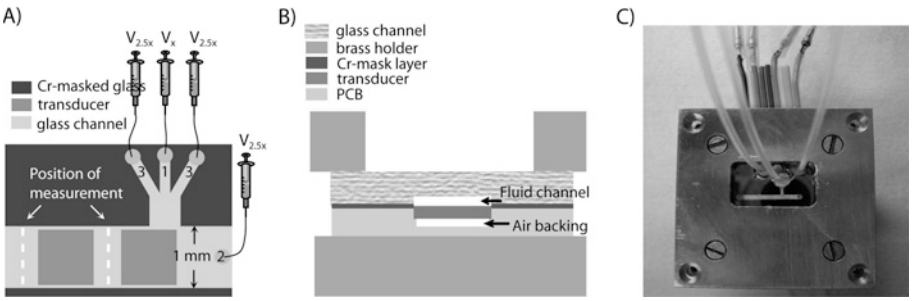

Figure 5-11. The platform with the Cr-masked glass and the underlying PCB layer with integrated transducers and electrical interconnects; A) schematic, B) cross-sectional view and C) photo.

The main part of the mixing, 80 %, occurred within 0.36 s and the mixing was completed after additional 0.72 s, *Figure 5-12A*. The mixing efficiency declined with increasing fluid velocity, but mixing was still evident at 85 μL min^{-1}.

Enhanced chemical lysis of *E.coli* K12 cells was demonstrated in the device due to active fluid mixing.

An analytical expression was derived to qualitatively describe the phenomenon. Theoretical description of the radiation force has earlier been presented by Rozenberg,[38] however for a density interface *perpendicular* to the wave propagation direction. For multiple number of interfaces, i, of area $A_{interface}$, in a standing wave in the z-direction between rigid boundaries, the

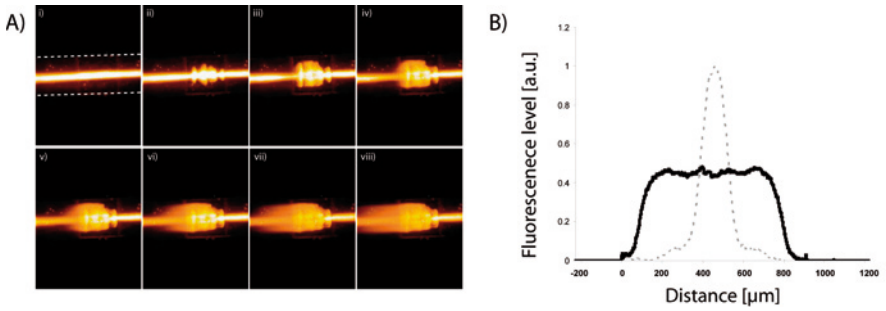

Figure 5-12. A) A sequence of images of the distribution of the fluorescently labelled middle flow above the mid-channel transducer. The flow direction is from right to left. The fluorescent sample flow is of lower density compared to the sheath flow and the total fluid volume has a velocity of 0.7 mm s^{-1}. The time interval between each image (i-viii) is 60 ms. B) The intensity profiles across the fluid channel 500 µm down stream the mid-channel transducer, before (dotted grey) and after (black) transducer activation at a driving frequency of 10.3 MHz and a total fluid velocity of 0.7 mm s-1

total interface radiation force, here F_r, can be expressed

$$F_r(z) = i \cdot A_{\text{int}\,erface} Q_{SW} \frac{\left\langle \left| v_t^2 \right| \right\rangle}{2} \cos^2\left(\frac{2\pi}{\lambda/2} z \right) \left(\rho_{01} - \frac{Q_2}{Q_{SW}} \rho_{02} \right) \qquad (13)$$

where λ is the wavelength of the acoustic wave and v_t, is the velocity amplitude at the transducer interface. The pressure amplitude in the layer depends on the quality of the cavity resonance, Q, which in turn depends on the density of the fluid since it affects the wavelength. For water the Q is denoted Q_{SW} and is obtained from electrical measurements. The Q-value for the non-matched fluid, Q_2, is approximated by a Gaussian function.

The above expression assumes stepwise density difference at an interface and the force will be reduced as the density difference decreases due to the convective motions caused by the radiation force.

For a standing wave in the channel, *Figure 5-13*, the top and bottom layers are expected to experience the highest force, according to *Equation 13*. The force is directed towards the denser material. Due to the conservation of mass flow, a flow in the opposite direction is expected to occur in the middle region where the radiation pressure is weaker.

The analytical expression is plotted in *Figure 5-14* together with measurement data. The high-density middle fluid is varied between 0-4.5 % density difference relative water. At zero density difference no mixing was observed, clearly separating this mixing mechanism from the acoustic mixing observed in a homogenous fluid. Compared with mixing induced by acoustic streaming, it is advantageous that the mixing is not caused by acoustic ab-

sorption losses, especially when temperature increase in the channel is critical. The analytical expression is in agreement with the measurement data.

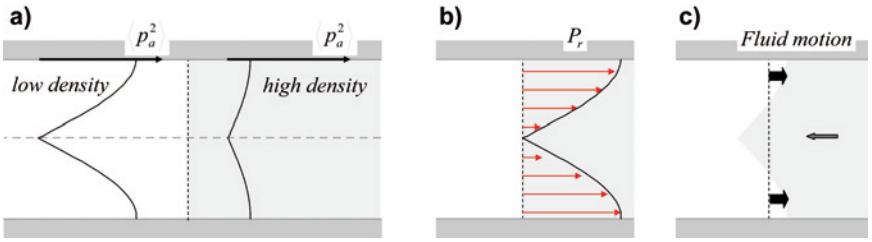

Figure 5-13. The principle of the mixing by radiation force at a density interface in a standing wave is illustrated. a) The time-averaged squared pressure amplitude in a standing wave at the interface between a lower-density fluid (white) and a higher-density fluid (grey). b) The radiation pressure at the interface which is parallel to the wave propagation direction, and c) the expected movement of the fluids at the interface due to the radiation force (black arrows) and due to conservation of mass flux (grey arrow).

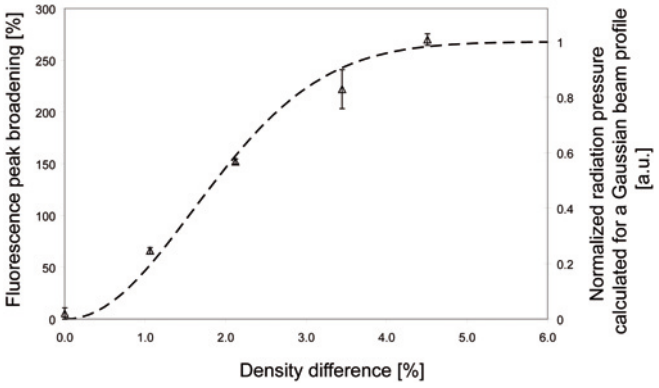

Figure 5-14. The measured fluorescence peak broadening (triangles) and the calculated radiation pressure estimation according to *Equation 13* (dotted line), as a function of the relative density difference between the two fluids. The density is assumed to increase linearly with glycerol concentration.

The second equation in the paper may need some extra comments. The mean pressure, p_a *(*Lagrangian radiation pressure*),* experienced by a particle equals the pressure at a fixed location, p *(*Eulerian radiation pressure*)*, plus an additional term, $\langle \rho v^2 \rangle$.[39] According to Hager[39] the Lagrangian coordinate system describes the individual fluid particles while the Eulerian describes the system at a fixed point in space, or equivalently the radiation pressure 'felt' by a fluid particle versus 'seen at a fixed point'.

5.3 MIT for µFACS

The Fluorescence Activated Cell Sorter (FACS) is standard equipment in bioanalytical laboratories for analysing and separating cell samples, *Figure 5-15A*. It enables single-cell analysis at very high speed (20 000 cells s^{-1}) with a very high degree of discrimination between different kinds of cells. However, it is expensive and requires skilled personnel to operate. Down-scaling the FACS and integrating with other steps offer many benefits.

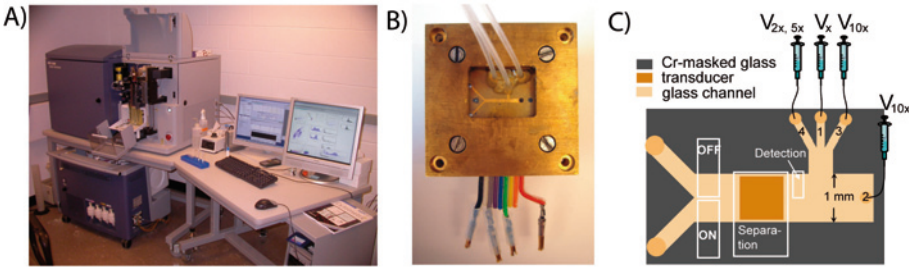

Figure 5-15. A) A commercial FACS, B) the MIT platform employed for µFACS and C) illustration of the fluidic set-up where the particles enters from the inlet (1), the flow (4) was the shuffle-flow with higher density and the flow (2) and (3) was used to position the interface relative the transducer surface.

The MIT platform was evaluated for µFACS application, in *Paper 5*, by exploiting acoustic radiation forces on a fluid-fluid density interface. The induced fluidic movement caused particles or cells on either side of the fluid interface to be displaced reproducibly sideways in the channel. To the authors knowledge it is the first time this method is described.

Relative other on-chip sorting methods such as hydrodynamic, dielectrophoretic and optic sorting the robustness, gentleness of acoustic forces in addition to their flexibility regarding the cells and the cell medium is emphasized.

The set-up is shown in *Figure 5-15C* where the flow (4) has higher density and is labelled 'shuffle flow' since its movement relative to the sample fluid interface causes displacement of the particles that enters from the sample inlet (1). The other flows are used to position the density interface relative the acoustic field above the transducer. A cell-friendly shuffle fluid can be used, for instance Dextran. The driving voltage at the transducer was 8 Vpp or lower.

At constant transducer activation the system was shown to accomplish up to 700 µm sideways displacement of 10 µm beads in the 1 mm wide channel, *Figure 5-16*. This is much larger than if utilizing the acoustic radiation force acting directly on particles, where the limitation in maximum displacement is between a node and an anti-node which at 10 MHz is 35 µm. Large displacement is desirable for sorting since it enable less strict requirements on the fluidics at the outlets.

In addition, separating several kinds of particles in a sample is possible by deflecting particles into multiple outlets by applying different voltage levels to the transducer. Thirdly, the large displacements enable the use of a low voltage signal, thereby minimizing the temperature increase in the channel.

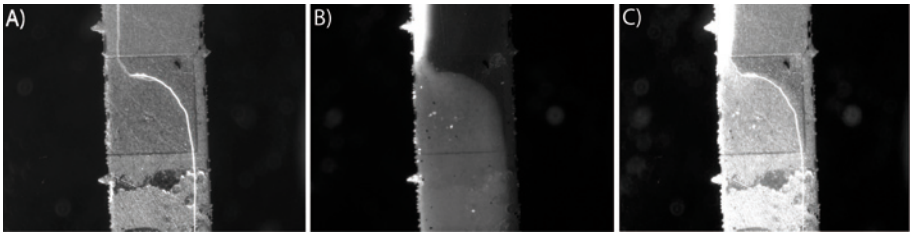

Figure 5-16. A) Particle trajectories of fluorescent 10 µm particles at a total flow velocity of 1.6 mm s^{-1} during continuous transducer activation, B) fluid distribution of the fluorescently labelled higher-density shuffle flow and C) the two superimposed images for comparison.

The particles motion in the acoustic zone above the transducer is illustrated in *Figure 5-17*. The acoustic radiation force initially acts on the particles in axial direction, causing alignment in the vertical direction. If this pre-focusing is not strong enough to enable positioning of the particles at a single vertical position in the initial stages of the fluid movements, the particles will not be displaced the same amount. A weaker pre-focusing (z-direction) is observed for smaller particles, as well as for particles with low acoustic contrast factor and for higher fluid flows (i.e. shorter residence times above the transducer). An initial acoustic focusing step can be added to enable the sorting of such particles.

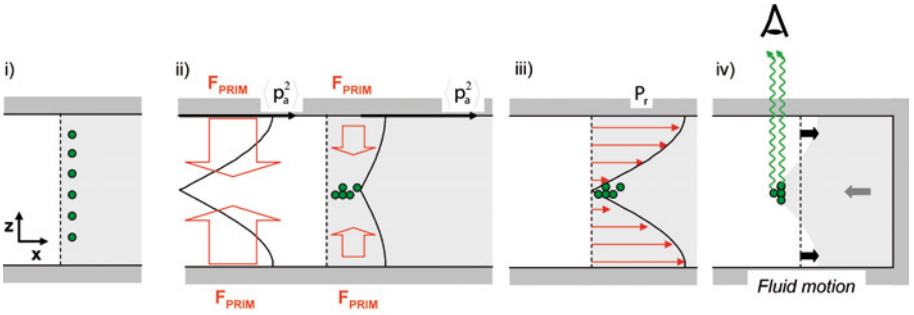

Figure 5-17. Illustration of the motion mechanisms for particles with high acoustic primary radiation force is shown. (i) The initial position of particles relative an interface between a lower-density fluid (white) and a higher-density fluid (grey), (ii) the time-averaged squared pressure amplitude in a standing wave and the primary radiation force that moves the particles to a pressure nodal plane in the middle of the channel, (iii) the radiation force acting on the interface and (iv) the expected initial displacement of the fluids and the displacement of particles due to the radiation force (black arrows) and due to conservation of mass flux (grey arrow).

A sorting speed of 27 cells s^{-1} was obtained for 220 µm cell displacement, for constant transducer activation assuming sample concentration of exactly one cell above the transducer at any time. A lower level of displacement was observed for higher flow velocities. Based on the time for maximum fluid displacement in *Paper 4*, the switch time was measured to 0.36 s corresponding to a sorting speed of approximately 3 particles s^{-1}.

Automatic switching was performed by the use of a Labview software program (8.2.1, National Instruments) controlled by the fluorescence signals from detected cells. In the automatic evaluation, a speed limitation of 0.3 s existed for the operation of the function generator. In the automatic sorting of every second cell, the system was demonstrated to sort single cells with high success rate, *Figure 5-18*.

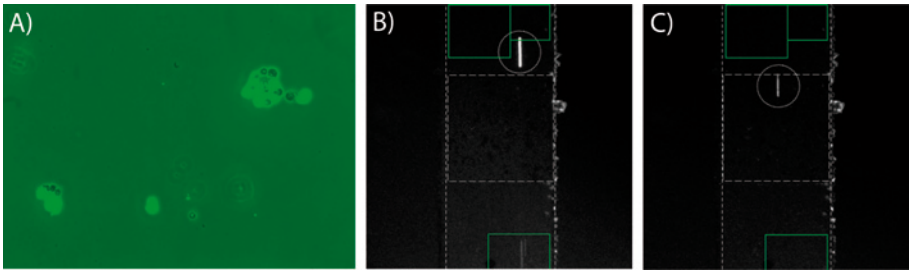

Figure 5-18. The µFACS-system was tested with E-GFP expressing β-cells, which are insulin producing cells. (A) About 50 % of the cells were expressing the fluorescence with slightly different intensities. (B) Images from the software program controlling the automated system showing a non-sorted β-cell and (C) a sorted β-cell.

The demonstrated ability to sort biological single-cells makes the presented µFACS system suitable in applications for sorting or preconcentration of cells in relatively small sample volumes and several applications were suggested in *Paper 5*. The gentleness of the acoustic switch makes it especially useful in applications for mammalian cells where viability in the following step is required, such as in transplantation.

5.4 IDT for non-labeled sorting

5.4.1 The Inter Digital Transducer (IDT) excitation

Surface acoustic waves (SAW) generated by inter digital electrodes (IDE) were used in a sorting platform at 35 MHz, in *Paper 6-8*. The SAW-excitation is expected to generate many advantageous properties for the particle manipulation devices. Compared with the PZT, the Lithium Niobate ($LiNbO_3$) and Lithium tantalite ($LiNbO_3$) are associated with low material losses and hence do not significantly contribute to any temperature increase in the fluid. The viscous absorption in a water layer of 100 µm is less than 1 permille at 10 MHz, and even though it is several times larger at 40 MHz it is still less than 1 %, which therefore is not expected to increase the temperature much. The IDT enable a planar design and easy inspection by being positioned outside the channel region, *Figure 5-19A*. Furthermore, the IDT enables the use of a higher driving frequency than usually employed for acoustic particle manipulation and thereby stronger acoustic forces at a certain acoustic pressure level. Potentially, the manipulation of smaller particles is enabled by increasing the frequency.

The large aperture of the IDT relative the wavelength enables a uniform excitation along the channel and little divergence of the acoustic field and therefore potentially a uniform acoustic field in the channel, which is advantageous for avoiding excitation of acoustic streaming and spurious cavity modes.

The acoustic pressure level inside the channel depends on a number of factors; the electromechanical coupling and losses of the piezoelectric material, the quality factor of the transducer design which amplifies the response, coupling into the fluidic channel, further signal amplification by resonance in the channel and the fluid layers and on the electrical matching relative the function generator. Compared with the PZT, the $LiNbO_3$ and $LiTaO_3$ materials display considerably lower electromechanical coupling but also lower losses, see *Appendix D*.

The transducer structure employed consists of IDT strips and reflector structures positioned on the outer side of the IDTs, *Figure 5-19B*. The frequency of operation is determined by the sound velocity divided by the wavelength as defined by the electrode period of 96 µm. 120 IDT electrode strips were used and were organized into 40 pairs of one wavelength with potential (++-). The spacing and width of the electrodes are 1/6 wavelength which makes them non-reflecting since no energy is trapped underneath the electrode structure. The reflector strips are positioned at the outer side of the IDTs and have a quarter wavelength spacing and width which enables unidirectivity of the radiated acoustic wave, since the waves reflecting at the electrodes edges interfere constructively.

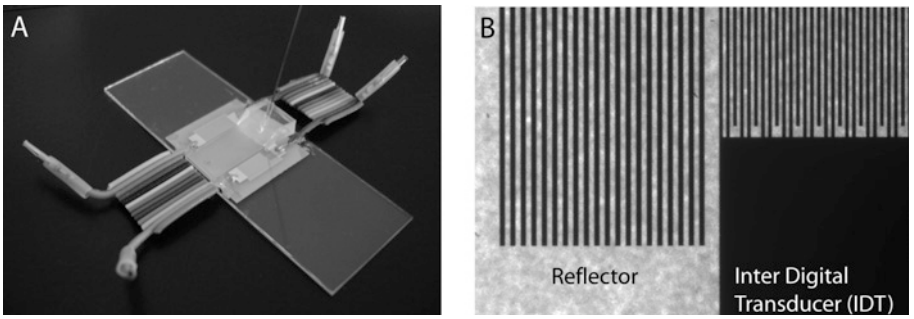

Figure 5-19. A) System set-up with the gold IDT structure on the frosty one-side polished lithium tantalite substrate mounted on a microscope glass slide. A fluidic inlet is provided by a glass capillary and a PDMS fluidic connection. The electrical connections can be operated as a single IDT or two IDTs in series. B) Close-up of the IDT strips and the reflector strips.

5.4.2 SAW-excitation in a PDMS channel

A device for acoustic manipulation in the 40 MHz range was evaluated for a 50 µm wide PDMS channel. Unidirectional interdigital transducers on a Y-cut Z-propagation lithium niobate wafer were used to excite a surface acoustic wave that generated an acoustic standing wave inside the microfluidic channel.

The high frequency employed requires small channel width since the wavelength is short. To be able to exploit the particle alignment in a narrow channel without very narrow fluid-outlet channels, a modified trifurcation flow-split outlet design as shown was evaluated. Two channels were evaluated. Alignment of 1.9 µm polystyrene particles, *Figure 5-20B,C,* and fat particles, *Figure 5-20A* was observed into pressure nodes and pressure anti-nodes respectively. For a speed of sound in water of 1500 m/s the wavelength in water at 39 MHz is 38 µm, hence the channel width of 50 µm encompasses approximately 1.3 wavelengths.

Difference in node position relative the channel wall is expected for different devices, since the acoustic path length will vary between different devices depending on the exact position of the PDMS channel.

The result of the inter-node spacing corresponding to the wavelength in water is different from IDT-excitation into a PDMS-channel presented elsewhere[85] and into a cavity without side-walls[86] where the inter-node distances were larger. The here observed inter-node distances are the same as generally observed for BAW-excitation in glass channels.[87, 88] The difference between these experiments could possibly be explained by the coupling of the SAW into the PDMS. In our case we expect a strong coupling due to our bonding process. It is then expected that the BAWs generated by refraction

of the SAWs from both sides of the PDMS-structure interfere and create a standing BAW in the PDMS layer including the channel.

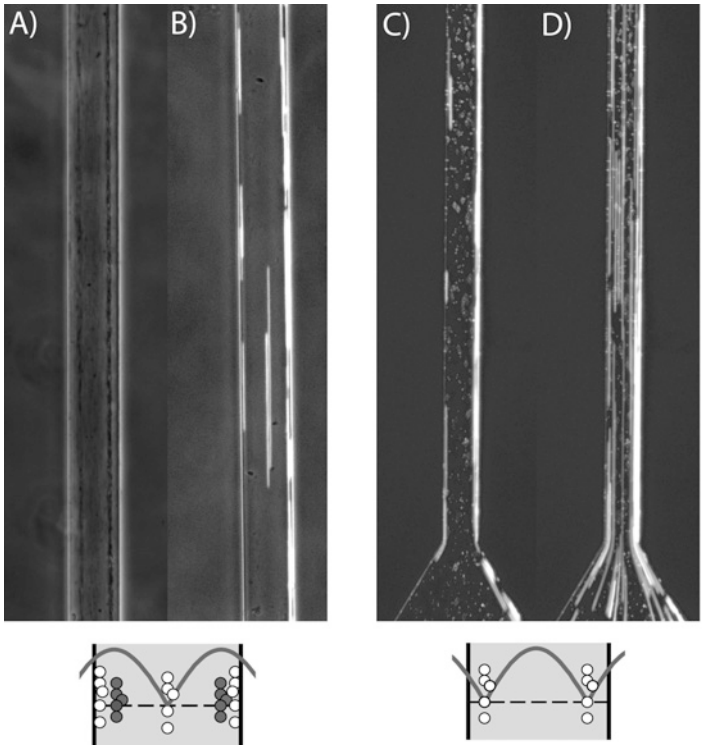

Figure 5-20. Alignment for the 38.9 MHz-device of A) fat particles (negative acoustic contrast factor) and B) 1.9 µm polystyrene beads (positive acoustic contrast factor). The fat particles (dark) are observed to align into two lines positioned some distance from the walls, while the polystyrene beads (white) align into three lines positioned at the walls and the channel middle (flow speed of 0.03 µL/min). For an equivalent channel, the 39.1 MHz-devices C) the alignment of the 1.9 µm polystyrene beads is observed to occur into two nodes and D) OFF (flow speed of 0.05 µL/min, 20 mms^{-1}). The illustrations show the expected pressure amplitude and the alignment positions for fat particles (dark) and polystyrene beads (bright).

Channel resonance at a frequency with pressure-nodes at the channel wall is opposite to the case normally observed for the high acoustic impedance channel walls.[88] A half wavelength channel with pressure-nodes at the channel walls is beneficial in some applications. For instance, when negative acoustic-contrast-factor particles to be sorted causes clogging if in direct contact with the channel wall and the use of sheath flow is not advisory due to dilution of the remaining fluid. One such application is the removal of fat particles in milk samples before performing bacterial analysis.[57] If contact with the channel wall is not an issue, the removal of positive-θ particle can be more efficient if the particles are exerted through two side-outlets instead

of one middle outlet. Removal of high concentration blood cells in plasma-purification could possibly be one such application and where the yield of the remaining medium is critical.[89]

An angular off-alignment of the channel relative to the pressure nodes was observed for the 38.9 MHz-device and can be used for positioning all particles very close to one of the channel walls, as illustrated, *Figure 5-21*. Applications may be positioning of coated-beads or spores to sensor surface.[90]

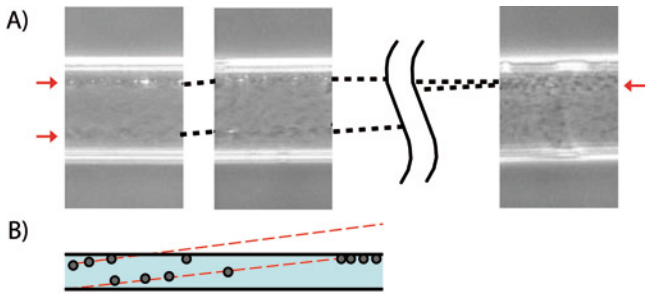

Figure 5-21. An off-alignment of the 50 µm channel relative to the IDTs generated asymmetric alignment of the particles in the channel. A) The alignment of fat particles upstreams in the channel is observed to occur into two nodes (arrows) (flow velocity of 0.03 µL/min, 12 mm/s). Further down the channel the position of the nodes relative the channel walls was shifted (dotted black line). At the channel outlet, this effect caused alignment of all particles to one of the channel walls. B) Schematic showing that the channel misalignment relative to the pressure nodes can be used for positioning particles very close to one of the channel walls.

5.4.3 SAW-excitation in a glass channel

The work in *Paper 7* extends the use of SAW for acoustic manipulation from exclusively in PDMS channels to also include glass channels. While the PDMS material is ideal for fast prototyping and bonding to silicon-based materials the hydrophobic surface of native PDMS may be less advantageous than glass both for filling the channel and for surface interactions between the sample and the channel walls. Further, it is expected that the SAW will be coupled into the channel structure both for the PDMS and the glass channel. Due to low absorption in glass, this structure will be able to more efficiently transport the coupled wave to the fluid layer and also allow energy build-up in the glass structure.

The borosilicate channel was wet etched to a channel width of 60 µm and a depth of 25 µm. Bonding of the borosilicate glass and lithium niobate substrate was performed on chip-level by an adhesive SU8-5 layer.

The alignment of 1.9 µm polystyrene beads occurred into three nodes, at the channel middle and the channel edges, *Figure 5-22*. For a speed of sound

in water of 1500 m/s the wavelength in water at 36.5 MHz is 41 µm, hence the channel width encompasses approximately 1.5 wavelengths or three nodes.

The node-spacing is equal to what is generally observed in BAW-transducer systems and different from what is obtained for some SAW-transducer systems with PDMS-channel[85] or without side-walls[86]. This observation, in addition to the possibility of single-IDT operation, supports the glass structure as the main origin of reflections rather than counter-propagating waves from the two IDTs. The possibility of operation with only one transducer makes the total device smaller.

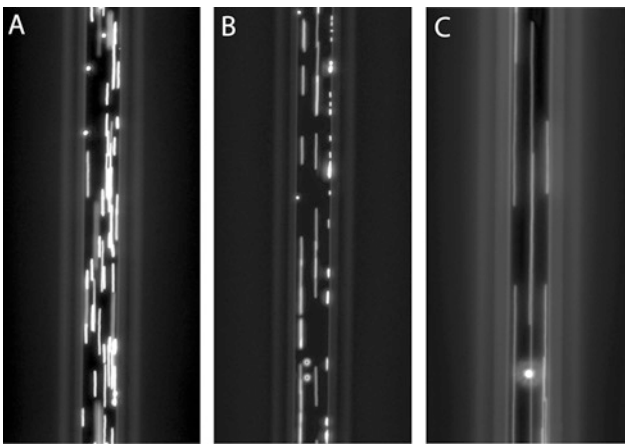

Figure 5-22. Position of the beads in the 60 µm wide channel for A) transducer off, and B) for single-IDT operation and C) the two IDTs operated in series.

5.4.4 Interface Acoustic Wave coupling – manipulation of sub-micrometer particles

In *Paper 8,* we present an acoustic manipulation device where the acoustic excitation occurs by surface acoustic waves (SAW) and where the coupling of energy into the channel occurs by an acoustic interface wave (IAW) which is expected to enable efficient coupling of the energy into the micro-fluidic channel.

IAWs or Stoneley waves propagate without losses along an interface between two solid media, but arise only in specific combinations of materials and propagation directions. In this system a 34 MHz SAW propagating in the Z-direction on the surface of an X-cut $LiTaO_3$ were coupled to a Stoneley wave propagating at the $LiTaO_3$/silicon dioxide interface.

The utilization of high frequency in addition to efficient coupling of the energy into the channel by IAW is anticipated to generate efficient particle manipulation. Acoustic manipulation of submicrometer polystyrene particles

in continuous flow microchannels is not commonly reported in literature. Biologically interesting particles, such as bacteria and viruses, are found in this size range.

Higher radiation forces enable manipulating of smaller particles, unless manipulation is prevented by acoustic streaming. The kind of acoustic streaming that is expected to influence the alignment the most is the Rayleigh streaming, where the streaming velocity in the radial direction (where the maximum velocity is observed) is proportional to the frequency.[38] Hence, according to theory using a higher frequency would not necessarily enable the manipulation of smaller particles. However, if acoustic streaming is avoided, the size of particles possible to manipulate is extended.

The channel was fabricated by wet etching silicon dioxide wafer to a channel depth of 40 µm and a width of 120 µm. The glass channel was adhesively bonded to a 500 µm lithium tantalite wafer by a thin SU-8 layer.

Particle alignment of 0.5 µm polystyrene particles was demonstrated at 34.7 MHz into one node in the 100 µm wide channel, *Figure 5-23*.

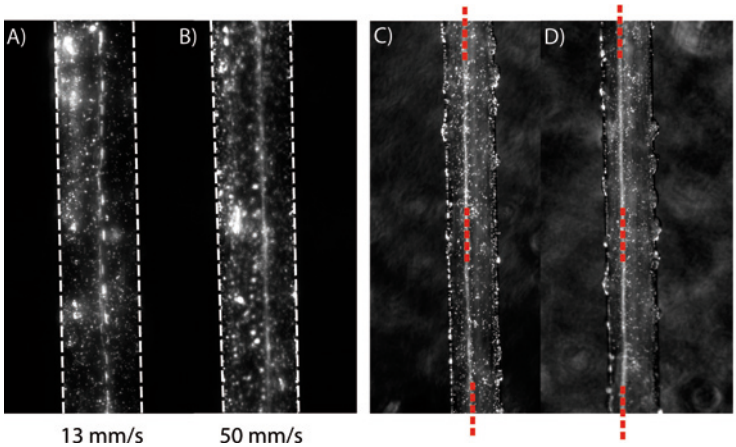

Figure 5-23. Alignment of 0.5 µm polystyrene beads into one node in the middle of the 100 µm wide channel, A-B) at two different flow velocities. Particles sticking to the channel walls is observed as round spots as oppose to the lines obtained from moving particles. Alignment C) parallel to the channel walls as observed for single-IDT operation or B) off-aligned to the channel walls as observed for some of the frequencies for series-IDT operation. Though a waviness of the channel wall was observed for some channels at some parts of the channel, at continuous flow these effects were smeared out.

Acoustic streaming and spurious cavity modes are found to be suppressed, as observed at zero fluid flow. The operation by two IDTs was found to influence the position of the alignment nodes, *Figure 5-23D,* indicating the influence of counter-propagating waves from the two IDTs as opposed to energy build-up in the channel structure. The inter-node distances observed exceed the approximately 40 µm expected for water but were in

agreement with previous reports for standing SAWs in PDMS channels[85] and in cavities without side walls[86].However, the internode distances do not appear sufficient for the determination of the interference mechanisms creating the manipulation forces. The relative large inter-node distance is advantageous for continuous-flow operation since it enables integration with a simpler flow split design and does not require very narrow channels.

5.5 Concluding remarks

Acoustic radiation forces enable non-contact, strong, gentle and label-less or labelled manipulation of particles and fluids. The initial work in this thesis regards a platform for acoustic trapping at localized acoustic zones by miniaturised integrated transducers (MIT). The thermal management of the platform was evaluated and showed that the temperature increase is moderate for the small transducers provided that the operational frequency is selected wisely.

The platform was also employed for mixing of fluids at a density interface, which is a method that is well suited for microfluidics but has not been previously employed. The MIT-platform was also demonstrated for a new method of moving particles by acoustic radiation forces, for application in fluorescence activated cell sorting.

In the second platform, interdigital transducers (IDTs) were used to excite a surface acoustic wave that generated an acoustic field in a PDMS channel, glass channel and silicon dioxide channel. Several general advantages are found for IDTs regarding the strength of the radiation force for higher frequency, the thermal management, the planar design and the easy inspection. The PDMS device enabled flexibility regarding the node positions and demonstrated ability to position all particles to one channel wall. The glass device enabled energy containment in the glass structure and more hydrophilic and stable surface properties of the channel. The interface-wave device enabled submicrometer polystyrene particle manipulation in continuous flow with favourable internode spacing. The IDT platforms display high potential for future studies.

Appendix A: Theory Microfluidics

Fluids are characterized by the property of deforming continuously under the action of external shear forces.[91] Most water-like fluids are Newtonian fluids, *i.e.* the shear stress, τ, is linearly proportional to the gradient of the velocity, v, in the direction perpendicular to the plane of shear

$$\tau_x = \eta \frac{dv}{dy} \tag{A1}$$

where, η is the dynamic (absolute) viscosity. A *laminar* flow follows smooth predictable streamlines as opposed to a turbulent flow. The laminar property is one of the cornerstones of microfluidics since it allows transporting and performing operations sequentially in a predictable manner. At the microfluidics length scales, the fluid appears as continuous (distances > 0.3 nm). A 'fluid particle' is a small segment of the fluid, typically a volume of side length 10 nm, which is regarded as a unit and responds in a predictable manner to external stimuli.[91] The flow is laminar for a Reynolds number, *Re*,

$$\mathrm{Re} = \frac{\rho D_h}{\eta} u \tag{A2}$$

below approximately 2300. ρ is the density, u the flow speed and D_h the hydraulic diameter which for a circular channel geometry is the channel diameter and for a quadratic channel the channel side length. Reynolds number describes the ratio of the inertial forces relative the viscous forces.

For a pressure-driven flow, the pressure required to push the fluid in the channel, Δp, increases fast with decreasing channel size,

$$\Delta p = Q\left[\mu L / \min\right] \cdot \frac{12\eta L}{h^3 w} = v\left[mm / s\right] \frac{12\eta L}{h^2} \tag{A3}$$

for the flow rate Q, the channel length L, the viscosity η, the channel height h, and the channel width w, where $h << w$.[91] It is possible to calculate on microfluidic networks in equivalence of an electrical circuit. The pressure-driven flow, displays a parabolic flow profile which renders particles to

travel at different speed at different heights in the channel. Focusing the particles to the channel middle, for instance by acoustic forces, can alleviate this problem.

Mixing is often required in microfluidic applications and is performed by external force, *active mixing*, or by channel geometry, *passive mixing*. The mixing can be characterized by the convection relative the diffusion rate by the Pecelt number, *Pe*,

$$Pe = \frac{vd}{D} \tag{A4}$$

where d is the radius or width of the channel, v is the fluid velocity and D is the diffusion coefficient.[91] For high *Pe*-number, mixing is no longer limited by diffusion. D is in the range of 10^{-9} m^2/s (10 $\mu m^2/s$).

Forces on particles in microfluidics

When manipulating a particle in a flow, the motion of the flow relative the particle exerts a force on the particle, *Stoke's drag force*, $F_{S,x}$,

$$F_{S,x} = 3\pi\mu d_p \cdot u_x \tag{A5}$$

where μ is the fluid viscosity, d_p is the particle diameter and u_x the relative fluid velocity. The expression is valid for the assumptions of Re<<1 and the particle positioned several times its radius away from the channel walls.[91]

Particles in a microfluidic system will be subject to a buoyancy-corrected gravitational force,

$$F_B = \left(\rho_p - \rho_0\right) g V_p \tag{A6}$$

where g is the standard gravity, ρ_p is the density of the particle, ρ_0 is the density of the fluid and V is the volume of the particle. A particle with density lower than water will experience a lifting force.

For a cluster of particles interparticular forces arise, such as due to surface charges. As a result, particles may stick to each other which in a practical case is addressed by adding detergent to the fluid.

For very small particles, ≤ 0.1 μm, diffusion due to Brownian motion can become relevant as the mobility increases for smaller particles,[92] making these particles difficult to separate by acoustic forces.[79] Higatashani et al. calculated for particles with an acoustic contrast factor, Φ, (*see 2.2.2*) of 0.8 that the smallest particles possible to gather in a pressure node were of size 0.1 μm.[92]

Appendix B: Recent devices for acoustic manipulation

In the last two decades, ultrasound in fluidic systems for bioanalytical applications has received much attention. Generally, different system designs and sometimes signal modulation are employed, and specific applications are targeted. To illustrate the field, a selection of devices is shown in *Figure B 1* and several devices are reviewed below.

The frequency range that is most often employed is 1-10 MHz which allows for the generation of standing waves for channel heights in the range of 10 to 100 µm. The small channel size makes high fluid volume applications challenging, though parallelism in the microsystems can be used to increase the total volume. For instance, a flow of 500 µL/min has been obtained for an eight channel separator.[93]

Gathering of particles

Gathering of particles in a volume is performed by the acoustic standing wave in order to speed up their collision rates and thereby increase the speed and sensitivity of Latex Agglutination Tests (LAT) assays (see *1.3.1*). A set-up consisting of a tubular transducer with a vertical glass capillary inside, has been evaluated by LAT for virus detection,[94] *Figure B 1A*, and for bacterial detection[95, 96]. The device was operated in batch mode, gathering beads at the pressure nodes followed by sedimentation of the bead aggregates. In some cases, the use of ultrasound enabled a reduction of the test time and an increase of sensitivity by several orders of magnitude.[96]

For very high sensitivity in the reaction between bead and analyte in LAT, a low bead concentration is needed.[41] Ultrasound gathering of particles has therefore also been employed in the detection step, such as by concentration of beads in a 96-well plate by placing a transducer into the wells.[97]

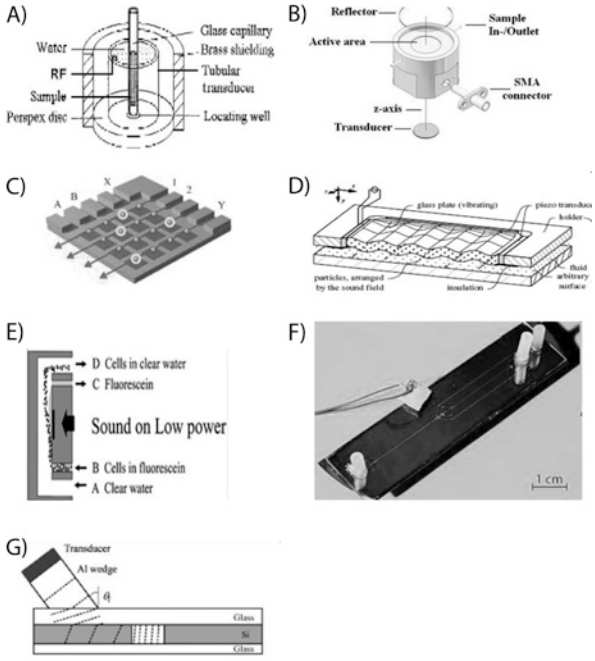

Figure B 1. Acoustic manipulation systems: **Trapping in lateral direction**: A) batch wise trapping and sedimentation (*With kind permission from Springer Science + Business media:*[94]), B) trapping for cell clusters (*Reprinted from* [33]*, with permission from Taylor and Francis*) ,C) Multiple miniaturized trapping spots for 'dynamic arraying' (*Reprinted from*[66]*, with permission from Elsevier*), D) multiple trapping spots by lateral mode in transducer[98]. (*With kind permission from Wiley InterScience*) **Sorting in axial direction**: E) medium exchange[99] (*Reproduced by permission of the Royal Society of Chemistry*), F) Externally positioned transducer [100] (*Reproduced by permission of the Royal Society of Chemistry*), G) by an wedge angle acoustic element[78] (*With kind permission from Wiley InterScience*).

Selective retention

Another acoustic standing wave operation is the selective retention in a continuous flow. For instance, a flow-through resonator placed over a cell culture reservoir has been used as a cell filter for protein production.[101] During continuous perfusion, the smaller protein molecules were able to leave the chamber while the larger cells where trapped and sedimented back into the chamber by gravitation of larger clusters. These chambers are rather large and flows of 0.7 L hrs^{-1} have been demonstrated.[102] The method has also been used for clarification of analyte.[80] For smaller chambers and lower flow rates, high clearance efficiencies of 99 % for yeast cells[103] and 80 % for bacteria[58] were obtained.

Alignment and subsequent separation by flow-split

Acoustic alignment and subsequent separation in a laminar flow by a flow split is employed in several systems. Such a system was presented by Yasuda.[104] Further examples are the stainless steel-brass device[105] and a water-cooled separator[79]. Different materials have been used; steel in the '*h-shaped separator*' and the '*Cardiff laminar flow filter*',[87] quartz-stainless steel,[99] *Figure B 1E*, and silicon-Pyrex[106]. Applications are for instance fluid clarification and cell medium exchange.

A different design, where external transducers positioned somewhere on the channel substrate and excite the entire channel substrate, has been exploited in several applications. The system has been combined with increasingly advanced fluidic design targeting several applications reviewed in the following.

In initial work a trifurcation outlet was employed, such as for removal of lipids in blood by shifting them to the channel edges.[107] The inverted approach of moving particles from outer streams into the middle stream enabled medium exchange for the removal of drugs and coagulation factor-contaminated plasma from red blood cells.[108] For protein assays, beads with bound antibodies were shifted into a clean buffer thereby separating them from the unbound antibodies present in the initial medium.[109]

By multiple channels in parallel increased throughput was demonstrated,[93] and a series setup enabled enhanced separation[100]. For multiple outlets 'Field Flow Fractionation' (FFF) simultaneous separation of several particles was demonstrated,[12] *Figure B 1F*. Modification of the fluid density by addition of cesium chloride (CsCl) was used to enable separation of equally-sized particles that were not otherwise separated.

Enhanced buffer exchange, for the application of biofunctionalized beads was addressed by a channel structure labeled 'side-washing' with a series of inlets on one side of the main channel, and a series of outlets on the other.[110] Initially, the particles and the medium were moved sideways in the channel by one side-inlet flow of new media whereafter particles were acoustically refocused into the channel middle.

Further applications for the principle design, include the removal of fat particles in milk for bacterial tests. To alleviate the problem of lipids clogging at the channel walls in a λ/2-channel an overtone and sheath flow was employed.[57] Furthermore, these systems are also employed for μFACS where one transducer enables 2D alignment in channel width region *1* and a second transducer enables binary switching in channel width region *2*.[111] Recently, high-purity plasma-cleaning at low driving voltage was demonstrated for a long meander-shaped channel.[112] To remove the high concentration of red blood cells, several out-of-plane outlets along the channel were used, and the number of cells was reduced 100 times.

Trapping

Cell trapping is another application for acoustic standing waves. Trapping for cell analysis in a cylindrical container with perfusion, known as the Cardiff mini-chamber,[81] *Figure B 1B,* has been employed in several studies. The principal set-up is a metal-container to which the transducer is docked. An example of the studies performed is the formation of dendritic or close-packed aggregations of eukaryote cells in response to different types of buffers.[14, 113] Other studies include the evaluation of the strength of a particle aggregate,[114] the cell-adhesion mechanisms in an aggregate of neural[115] and prostate[116] cells, and the aggregate formation and acoustic streaming[53, 117].

While the above trapping device relies on an acoustic gradient transverse to the wave propagation direction, another trapping device utilizes the radiation force parallel to the wave propagation direction.[118] By mounting a glass capillary through the transducer and the reflector plate, selective retention is performed to discriminate between two-particle-complexes and single particles in immuno-assay ELISA. This set-up was also demonstrated for increased speed of aggregation formation in LAT.[119]

Trapping has also been demonstrated by miniaturized integrated transducers (MIT) positioned in the bottom channel wall.[48]Apart from the work presented in this thesis, this system has been evaluated for bead assays and selective cell trapping for forensic analysis[120]. The MIT-platform of individually addressable trapping sites operated in series has been demonstrated for 'dynamic arraying',[66] and the extension to 2D-array has been outlined, *Figure B 1C* .

Multiple trapping positions has been demonstrated in a system by exciting lateral modes in a transducer plate[121] or a glass plate[122], *Figure B 1D*. The lateral excitation in the piezoelectric plate is performed by electroding only part of the plate.[123] These modes couple into the fluid, and the modes are contained in the fluid by a reflector.[124] Trapping in a 2D pattern along the channel has been demonstrated for one single wedge transducer at zero flow.[125] Recently, 2D-alignment into 456 nodes in a droplet was demonstrated by two orthogonal interdigital transducers.[126] The alignment of as small as 0.5 µm polystyrene beads was demonstrated.

Other operations

Other operations performed in acoustic standing wave systems include alignment for combination with optical tweezers[127] and positioning for sheatless focusing in cytometry by positioning a transducer on a glass capillary[128, 129]. In addition, enrichment of particles to a surface has been demonstrated for sensing applications[90, 130] by using close to a quarter-wavelength instead of a half-wavelength channel height[67]. A few systems exploit force-balancing of the acoustic force with electrostatic forces[131] or dielectric forces[132, 133] in order to manipulate on a smaller scale and in additional direc-

tions. Acoustic streaming has been employed for mixing fluids[55] and for fluid transport by travelling waves[134].

Transducer principles

The wave excitation has for some time most commonly been performed by bulk acoustic waves (BAW) where the transducers are positioned directly in contact with the fluid, or are separated by a coupling layer. In the latter case, the transducer can also be positioned further away from the fluid channel.

The bulk PZT is usually bonded or clamped to the channel structure. The multilayer PZT deposition by thick film processing onto the coupling layer has also been performed.[82] By using an external transducer, the possibility of disposing only the channel structure arises.

Additionally, acoustic energy can be coupled into the fluid by a wedge transducer,[132] *Figure B 1G*. By using several wedge transducers, simultaneous manipulation in several directions at different parts of the device has been demonstrated.[125] The pressure wave in the fluid can be split in two orthogonal directions,[125] and the wedge is observed to give rise to a 3D acoustic pattern in the channel. By using different channel geometries, the radiation forces can be localized further , as for a quadratic cavity[135]. The geometry of the channel can also be used to shape the field, such as focusing by a circular cavity.[136] Transitions from wider to narrower channels allow for the merging of alignment nodes, and hence for sequentially focusing particles into a narrow stream for comparably large fluid volumes.[137]

In addition to bulk transducers, excitation by interdigital transducer (IDT) has recently been demonstrated to enable particle alignment in a PDMS channel.[64, 85] The set-up enables operation at higher frequencies (in the range of 40 MHz).

Transducer structuring and signal modulation

Specific shaping of the acoustic field can be performed by transducer design and by signal modulation. A transducer design of two concentric piezoelectric elements arranged coaxially, has been employed to eliminate the acoustic side-lobes leading to an increase in the lateral energy gradients.[138] A circular signal electrode has been used on a square transducer to define the aperture and hence the acoustic field.[14] Asymmetric excitation of a piezoelectric transducer has been employed to generate only one pressure node in the lateral direction in a fluid cavity that is wider than $\lambda/2$.[127]

Shaping the acoustic field by signal modulation has been employed to suppress spurious cavity modes by frequency modulation.[139] A sequential change in frequency has been used to shift the position of the acoustic pressure nodes to transport trapped particles between nodes. This can be useful for non-perfusion cell analysis of non-diluted signaling molecules.[56, 140] Alternating between multi-node and single-node frequencies has been employed to separate particles based on their response time.[141]

Appendix C: Acoustic radiation forces cont.

The radiation force in the axial direction in a plane standing wave, F_{prim}, is expressed

$$F_z = -\frac{d}{dz}\langle U \rangle = \ldots = \left(\frac{4\pi r^3}{3}\right) p_0^2 \frac{\pi}{2\rho_0 c_0^3} f\left(f_1 + f_2 \frac{3}{2}\right) \sin\left(2\pi \frac{z}{\lambda/2}\right) \qquad \text{(C1)}$$

Hence, the radiation force is proportional to the driving frequency. The direction of the radiation force in a standing wave cavity is illustrated in *Figure C 2*, For multiple particles in a standing wave, secondary acoustic forces, *Fsc*, occur additionally due to the scattering of the incident wave on the other particles present in the trap. The secondary acoustic forces are short- range and will act to attract the particles present in the nodal plane.[142]

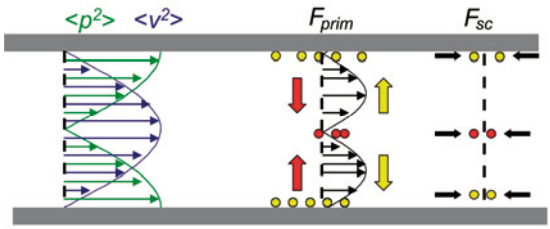

Figure C 2. Illustration of the time-averaged pressure amplitude (green) and the oscillation velocity amplitude (blue). The primary acoustic radiation force, F_{prim}, causes stiff and heavy particles (red) to move to the pressure node (red arrow) while the compressible and light particles (yellow) move to the pressure anti-node (yellow arrow). The secondary acoustic radiation force, F_{sc}, influences the particle behavior only at short distances such as when the particles are gathered in the nodal planes.

Force estimation

Numerical values of the acoustic force can be obtained, provided that the pressure amplitude or the velocity amplitude is known.

The stroke of a BAW transducer, U_0, can be estimated as the piezoelectric material constant d_{33} ($3*10^{-10}$ m/V) times the driving voltage (5 V) yielding a value of 1.5 nm. This displacement amplitude excites a pressure wave in the fluid.

The velocity amplitude of the wave, *v*, can be estimated by assuming that the wave is constructively interfering *Q* times (where *Q* is the *Q*-factor in the fluid cavity) by the expression $v \approx U_0 Q 2\pi f$. Hence, for 10 MHz the velocity amplitude is approximately 3 m/s. Assuming a plane wave, and considering the whole volume,[38] the pressure amplitude is 4.5 MPa for a density of 1000 kg/m^3 and a speed of sound of 1500 m/s. At this pressure level, the radiation force in the axial direction for a 5 μm polystyrene particle at 10 MHz is 80 pN and 680 pN for a 10 μm particle.

Appendix D: Electro-mechanical parameters

The *electro-mechanical coupling coefficient*, k, describes how much of the electrical energy supplied, W_{electr}, is transformed into mechanical energy, W_{mech}, for a certain mode

$$k^2 = \frac{W_{mech}}{W_{electr}} = \frac{d^2}{s^E \varepsilon^T} \tag{D1}$$

where d is the piezoelectric strain coefficient, s is the mechanical compliance, equal to $1/Y$, and ε is the dielectric constant.

High values of the electro-mechanical coupling coefficient is obtained for PZT ($Pb_xZn_{(1-x)}O_3$), especially for piezoelectrically soft PZT. Lithium niobate ($LiNbO_3$) and lithium tantalite ($LiTaO_3$) display considerably lower electromechanical coupling, *Table 1.*

Table 1. Typical values of material constants for BAW in PZT and some propagation directions employed in $LiNb0_3$ and $LiTaO_3$ SAW

	Cut	Propagation direction	k^2 [%]
PZT BAW	–	thickness	49
LiNbO3 SAW	Y	Z	4.9
LiTaO3 SAW	Y	Z	0.66

In resonant mode operation and for a certain geometry, an 'effective' coupling factor can be expressed[143]

$$k_{eff}^2 = \frac{f_p^2 - f_s^2}{f_p^2} \tag{D2}$$

where the frequencies are determined from electrical measurements. f_s is the frequency of maximum conductance (series resonance) and f_p is the frequency of maximum resistance (parallel resonance frequency).[143]

Material losses are usually divided into electrical and mechanical losses. The electrical loss factor, $tan\delta$, is defined as

$$\tan\delta = \frac{\varepsilon'}{\varepsilon''} \tag{D3}$$

where ε' and ε'' are the real and imaginary part of the permittivity, respectively. For lithium niobate and lithium tantalite, the dielectric losses are negligible. The mechanical loss, $tan\theta$, is expressed in terms of the mechanical quality factor, Q_M,

$$\tan\theta = \frac{1}{Q_M} \tag{D4}$$

Q_M-values are around 50 for piezoelectrically soft PZT, and 3000 for piezoelectrically hard PZT. For SAW materials the figure of merit $Q_M f$ is larger than 10^{13}, and Q_M is therefore very large for operation in the MHz range. A quality factor can also be used to characterize the resonance peak of a device,

$$Q_0 = \frac{f_0}{\Delta f_{FWHM}} \tag{D5}$$

where f_0 is the resonance frequency and the denominator, Δf_{FWHF}, is the width of the peak at half its maximum value.

The losses are defined in terms of how they are measured, rather than in terms of the loss mechanism causing it.[144] The loss factor that dominates most often for PZT is the domain wall motion. Non-180º-domain wall motion is associated with dielectric losses and dominates at low electrical fields. At high electrical fields, or for the large amplitudes obtained at resonance, the 180º-domain wall motion associated with mechanical losses dominates.[145]

Svensk sammanfattning

Avhandlingsarbetet handlar om design, tillverkning och utvärdering av miniatyriserade plattformar där man med akustiska krafter kan utföra flera av de operationer som är önskvärda för bioanalytiska system, så som fasthållande av celler, sortering av olika sorters celler, koncentrering av celler eller rening av vätska från partiklar. Den akustiska strålningskraften lämpar sig väl för att användas i de miniatyriserade och integrerade system vilka utgör ett teknikskifte för biomedicinska analyser och är ett stort tvärvetenskapligt forskningsfält. Typisk är den akustiska kraften på en partikel i dessa system 100 gånger starkare än gravitationskraften som partikeln upplever i vätskan!

Jämfört med storskaliga analyssystem kan flera fördelar vinnas genom miniatyrisering, och biomedicinska analyser kan komma att användas oftare, närmare patienten och för att lösa mer komplicerade frågeställningar. De provvolymer som behövs är betydligt mindre. Detta är en fördel när man vill analysera många kombinationer såsom vid screening för medicinsk diagnos, läkemedelsframställning eller forskning. Det är också en fördel vid frekvent mätning av visst värde i tex blod, där en liten provvolym utgör mindre obehag. Mindre mängd reagenser behövs också, vilket medför en kostnadsminskning. Analyserna går dessutom ofta fortare i mindre skala. Genom integrering av flera av de miniatyriserade operationerna på en plattform minskar behovet av arbetsintensiv förflyttning av proverna och minskar dessutom risken för smitta vid hantering av smittsamma prover.

Två plattformar har utvärderats i denna avhandling. Ett system där miniatyriserade ultraljudsgivare integreras i kanalbotten (Miniatyriserade Integrerade Transducrarna, MIT). Detta system lämpar sig för kvarhållande av celler, i en eller i flera punkter. Systemet är en bra för att studera celler utan påverkan av omgivande ytors egenskaper under kontinuerlig tillförsel av näringsämnen och bortförsel av skadliga bi-produkter. Detta system har utvärderats för temperaturökning i flödet under drift, viabiliten hos de infångade cellerna, akustisk kraft på en enskild partikel samt för optimal drivfrekvens.

Vidare har samma uppställning använts för att generera blandning av vätskor, en operation som inte naturligt sker i de små vätskekanalerna eftersom flödet är laminärt. Fenomenet av akustisk strålningskraft på vätskeytor har demonstrerats tidigare på makronivå. Principen skalar bra för användning i mikrosystem och vi har beskrivit effekten med ett analysiskt uttryck.

MIT-plattformen har också demonstrerats för att sortera celler individuellt i ett flöde aktiverat av en fluorescent signal, så kallad Fluorescens Aktiveras Cell Sortering (FACS). Principen för separeringen är att flytta cellerna genom att flytta en flödes-gränsyta med den akustiska strålningskraften. Storskaliga FACS är en standardutrustning i analytiska labb och en miniatyrisering ger flera fördelar så som direkt integrering med följande steg, enkel styrning utan speciellt utbildad personal, lägre pris och storlek därmed möjlighet till mer patientnära användning. Jämfört med andra micro-FACS i litteraturen kan framförallt framhävas den milda inverkan på celler som den akustiska manipuleringen innebär.

I den andra plattformen används en annan typ av ultraljudsgivare, kallade IDT (*eng.* Interdigital Transducers) och en annan typ av våg exciteras initiellt, en ytakustisk våg (eng. Surface Acoustic Wave, SAW). Flera fördelar finns med denna plattform så som låg temperaturökning, transparens och processning i plan. En högre drivfrekvens är möjlig för denna plattform, vilket innebär att starkare akustisk kraft påverkar partiklarna för ett visst akustiskt fält i kanalen. Applikationen är sortering av omärkta celler och partiklar i kontinuerligt flöde.

I artiklarna testades en silikon-gummi kanal, en glaskanal och en kiseldioxid-kanal. Olika egenskaper kan observeras och val av kanalmaterial bestäms generellt flera parametrar. För kiseldioxid-kanalen valdes en speciell materialkombination och vågpropageringsriktning för att stödja en gränsvåg (*eng.* interface wave eller Stonley wave) mellan kiseldioxidkanalen och det piezoelektriska substratet, vilket möjliggör effektiv koppling av den akustiska energin in till vätskan. Linjering av polystyren-partiklar med 0.5 µm diameter demonstrerades, vilket inte vanligen rapporteras i akustiska miniatyriserade sorteringssystem. Linjeringen skedde till positioner i kanalen med förhållandevis långt inbördes avstånd, trots den höga drivfrekvensen, vilket gör att denna metod lämpar sig väl för separering i kontinuerligt flöde med enkel fluidlikdesign.

Acknowledgements

I would like to acknowledge the ultrasonic network USWNet for arranging open and inspirational discussions in the field of acoustic manipulation. Thanks also to many of its participants for writing very nice theses!

I'd like to thank my supervisor Stefan Johansson for initially suggesting me to work at the university when I visited his company for an employment interview and I appreciate his faith in me throughout this time. I hope that I have learned to think 'micro' as I think that he does, though I know that I've not yet learned to think 'piezo' as he does. I am thankful to Tobias Lilliehorn for introducing me to this research field and for his inspirational personality! Special thanks to the head-of the department, Jan-Åke Schweitz, for looking after me as he does all PhD Students.

I am thankful to Mikael Evander for our collaboration and for making sure I've spent a wonderful time playing innebandy, holiday in Southampton and a frightful climb to the top of Besseggen. I acknowledge the fantastic duo of Thomas Laurell and Johan Nilsson and thank them for teaching me a lot and for adopting me as one of their own PhD-students whenever we meet at conferences etc.

I'd like to thank Sara Thorslund for nice collaboration and for sharing her wisdom regarding bioapplications. I am thankful to Ventsislav Yantchev for sharing his deep knowledge on wave propagation, and to him and Johannes Enlund for the fruitful collaboration in the SAW-projects. I appreciate Sara Thorslund, Zhigang Wu and Andreas Dahlin for sharing their knowledge on practical issues in microfluidics and many times supplying me with the appropriate particles, solvents etc.

I am thankful to Rosie Townsend for Novotny-Benez-modelling discussions and to Jeremy Hawkes for giving me access to their Novotny-Benes modelling program. I acknowledge Marcus Engholm for valuable discussions on modelling of piezoelectric material, especially in FEM. Thanks to Fredrik Lingvall for giving me access to their DREAM Toolbox simulation software and to Tadeusz Stepinski for allowing me to use their network analyser.

Thanks to Hanna Yousef for proof-reading this thesis.

I am thankful to Jonathan Bagge for solving all sorts of computer-related problems including keeping my lap-top running for five years! Thanks to Jan-Åke Gustafsson for the numerous times he has solved problems in the lab.

I also like to especially acknowledge some of my former and present colleagues and friends at Ångström lab: to Hanna for her most valued friendship on and off work, to the Tuesday-morning-swim-and-coffee team Micke and Sara, to Gunjana for her perspectives on life, to Marek and his talent for good jokes, to the fantastic Rullan lunch-team headed by Hugo and Kratz, to room-mate Niklas for discussions on piezo and life, to the people sharing conference-trip happenings such as meeting Madou, seeing NY, cow-bingo on a boat in Amsterdam, chasing hotels in Lyon, and to the crazy piezo-guys for good times such as skiing in half-pipes competing for a Jägermister!

To my family and friends outside the academic world for all the happy times!

Tack!

Linda

References

1. D. J. Beebe, G. A. Mensing and G. M. Walker, *Annu Rev Biomed Eng*, 2002, **4**, 261-286.
2. H. Andersson and A. van den Berg, *Sensor Actuat B-Chem*, 2003, **92**, 315-325.
3. S. M. Coward, C. Selden, A. Mantalaris and H. J. F. Hodgson, *Artif Organs*, 2005, **29**, 152-158.
4. F. A. Gomez, *Biological applications of microfluidics*, 1 edn., John Wiley & Sons, Inc., Hoboken, 2008.
5. T. Frisk, S. Rydholm, T. Liebmann, H. A. Svahn, G. Stemme and H. Brismar, *Electrophoresis*, 2007, **28**, 4705-4712.
6. A. Manz, N. Graber and H. M. Widmer, *Sensor Actuat B-Chem*, 1990, **1**, 244-248.
7. S. Haeberle and R. Zengerle, *Lab Chip*, 2007, **7**, 1094-1110.
8. R. Pal, M. Yang, R. Lin, B. N. Johnson, N. Srivastava, S. Z. Razzacki, K. J. Chomistek, D. C. Heldsinger, R. M. Haque, V. M. Ugaz, P. K. Thwar, Z. Chen, K. Alfano, M. B. Yim, M. Krishnan, A. O. Fuller, R. G. Larson, D. T. Burke and M. A. Burns, *Lab Chip*, 2005, **5**, 1024-1032.
9. German cancer research center, 20090314, http://www.dkfz.de/gpcf/24.html
10. F. K. Balagadde, L. C. You, C. L. Hansen, F. H. Arnold and S. R. Quake, *Science*, 2005, **309**, 137-140.
11. D. Jens, H. Stefan, L. Sascha, P. Sarah, S. Felix von and Z. Roland, *J Micromech Microeng*, 2007, S103.
12. F. Petersson, L. Aberg, A. M. Sward-Nilsson and T. Laurell, *Anal Chem*, 2007, **79**, 5117-5123.
13. C. H. J. Schmitz, A. C. Rowat, S. Koster and D. A. Weitz, *Lab Chip*, 2009, **9**, 44-49.
14. D. Bazou, W. T. Coakley, K. M. Meek, M. Yang and D. T. Pham, *Colloid Surface A*, 2004, **243**, 97-104.
15. D. Bazou, L. A. Kuznetsova and W. T. Coakley, *Ultrasound Med Biol*, 2005, **31**, 423-430.
16. J. El-Ali, P. K. Sorger and K. F. Jensen, *Nature*, 2006, **442**, 403-411.
17. N. Pamme, *Lab Chip*, 2007, **7**, 1644-1659.
18. E. Verpoorte, *Lab Chip*, 2003, **3**, 60N-68N.
19. J. C. Giddings, *Science*, 1993, **260**, 1456-1465.
20. L. R. Huang, E. C. Cox, R. H. Austin and J. C. Sturm, *Science*, 2004, **304**, 987-990.

21. M. Yamada, M. Nakashima and M. Seki, *Anal Chem*, 2004, **76**, 5465-5471.
22. K.-H. Han and A. B. Frazier, *Lab Chip*, 2008, **8**, 1079-1086.
23. M. Y. He, J. S. Edgar, G. D. M. Jeffries, R. M. Lorenz, J. P. Shelby and D. T. Chiu, *Anal Chem*, 2005, **77**, 1539-1544.
24. D. Bazou, W. T. Coakley, A. J. Hayes and S. K. Jackson, *Toxicol in Vitro*, 2008, **22**, 1321-1331.
25. E. Verpoorte and N. F. De Rooij, *Proceedings of the IEEE*, 2003, **91**, 930-953.
26. G. M. Whitesides, *Nature*, 2006, **442**, 368-373.
27. A. Kundt and O. Lehmann, *Annalen der Physik und Chemie*, 1874, **229**, 1-12.
28. J. W. S. Rayleigh, *The theory of sound*, Repr. edn., Dover Publ., New York, 1945.
29. M. Dyson, B. Woodward and J. B. Pond, *Nature*, 1971, **232**, 572-573.
30. W. J. Xie, C. D. Cao, Y. J. Lu, Z. Y. Hong and B. Wei, *Appl Phys Lett*, 2006, **89**, 214102-214101.
31. W. T. Coakley, *Trends Biotechnol*, 1997, **15**, 506-511.
32. T. Ryll, G. Dutina, A. Reyes, J. Gunson, L. Krummen and T. Etcheverry, *Biotechnol Bioeng*, 2000, **69**, 440-449.
33. D. Bazou, G. A. Foster, J. R. Ralphs and W. T. Coakley, *Mol Membr Biol*, 2005, **22**, 229-240.
34. J. Hultstrom, O. Manneberg, K. Dopf, H. M. Hertz, H. Brismar and M. Wiklund, *Ultrasound Med Biol*, 2007, **33**, 145-151.
35. M. Evander, L. Johansson, T. Lilliehorn, J. Piskur, M. Lindvall, S. Johansson, M. Almqvist, T. Laurell and J. Nilsson, *Anal Chem*, 2007, **79**, 2984-2991.
36. T. Kamakura, K. Yasuda and Y. Kumamoto, *Electron Comm Jpn 3*, 1999, **82**, 76-82.
37. H. Mitome, *Electron Comm Jpn 3*, 1998, **81**, 1-8.
38. L. D. Rozenberg, *High-intensity ultrasonic fields*, Plenum Press, New York, 1971.
39. F. Hager, Doctoral Thesis, Technical University of Vienna, 1991.
40. L. P. Gor'kov, *Sovjet Physics*, 1962, **6**, 773-775.
41. M. Wiklund and H. M. Hertz, *Lab Chip*, 2006, **6**, 1279-1292.
42. G. Whitworth and W. T. Coakley, *J Acoust Soc Am*, 1992, **91**, 79-85.
43. P. Brodeur, *Ultrasonics*, 1991, **29**, 302-307.
44. S. M. Woodside, B. D. Bowen and J. M. Piret, *Aiche J*, 1997, **43**, 1727-1736.
45. C. J. Schram, in *Sonochemistry*, ed. T. J. Mason, Royal Society of Chemistry, Cambridge, 1990, pp. 293-322.
46. L. E. Kinsler, *Fundamentals of acoustics*, 4. edn., Wiley, New York, 2000.
47. F. Lingvall and B. Piwakowski, *Dream Toolbox*, (2008), Uppsala.

48. T. Lilliehorn, U. Simu, M. Nilsson, M. Almqvist, T. Stepinski, T. Laurell, J. Nilsson and S. Johansson, *Ultrasonics*, 2005, **43**, 293-303.
49. R. J. Townsend, M. Hill, N. R. Harris and N. M. White, *Ultrasonics*, 2006, **44**, E467-E471.
50. S. M. Hagsater, A. Lenshof, P. Skafte-Pedersen, J. P. Kutter, T. Laurell and H. Bruus, *Lab Chip*, 2008, **8**, 1178-1184.
51. O. Manneberg, J. Svennebring, H. M. Hertz and M. Wiklund, *J Micromech Microeng*, 2008, 095025.
52. G. Hertz and H. Mende, *Zeitschrift für Physik A Hadrons and Nuclei*, 1939, **114**, 354-367.
53. J. F. Spengler, W. T. Coakley and K. T. Christensen, *Aiche J*, 2003, **49**, 2773-2782.
54. A. Hancock, M. F. Insana and J. S. Allen, *J Acoust Soc Am*, 2003, **113**, 652-659.
55. M. Bengtsson and T. Laurell, *Anal Bioanal Chem*, 2004, **378**, 1716-1721.
56. O. Manneberg, B. Vanherberghen, B. Onfelt and M. Wiklund, *Lab Chip*, 2009, **9**, 833-837.
57. C. Grenvall, P. Augustsson, H. Matsuoka and T. Laurell, µTAS 2008 Conference, Tokyo, 2008.
58. J. J. Hawkes, M. S. Limaye and W. T. Coakley, *J Appl Microbiol*, 1997, **82**, 39-47.
59. A. A. Doinikov, *J Acoust Soc Am*, 1997, **101**, 722-730.
60. A. A. Doinikov, *J Fluid Mech*, 1994, **267**, 1-21.
61. S. D. Danilov and M. A. Mironov, *Soviet Physics Acoustics*, 1984, **30**, 280-283.
62. S. D. Danilov and M. A. Mironov, *J Acoust Soc Am*, 2000, **107**, 143-153.
63. K. Yasuda and T. Kamakura, *Appl Phys Lett*, 1997, **71**, 1771-1773.
64. J. J. Shi, X. L. Mao, D. Ahmed, A. Colletti and T. J. Huang, *Lab Chip*, 2008, **8**, 221-223.
65. S. Kapishnikov, V. Kantsler and V. Steinberg, *J Stat Mech-Theory E*, 2006, P01012.
66. T. Lilliehorn, M. Nilsson, U. Simu, S. Johansson, M. Almqvist, J. Nilsson and T. Laurell, *Sensor Actuat B-Chem*, 2005, **106**, 851-858.
67. R. J. Townsend, M. Hill, N. R. Harris and M. B. McDonnell, *Ultrasonics*, 2008, **48**, 515-520.
68. X. H. Li, T. Abe and M. Esashi, *Sensor Actuat a-Phys*, 2001, **87**, 139-145.
69. L. Ceriotti, K. Weible, N. F. de Rooij and E. Verpoorte, *Microelectron Eng*, 2003, **67-8**, 865-871.
70. F. Niklaus, G. Stemme, J. Q. Lu and R. J. Gutmann, *J Appl Phys*, 2006, **99**, 031101.
71. M. Hill, *J Acoust Soc Am*, 2003, **114**, 2654-2661.
72. M. Hill, Y. J. Shen and J. J. Hawkes, *Ultrasonics*, 2002, **40**, 385-392.

73. M. Hill and R. J. K. Wood, *Ultrasonics*, 2000, **38**, 662-665.
74. H. Nowotny and E. Benes, *J Acoust Soc Am*, 1987, **82**, 513-521.
75. H. Nowotny, E. Benes and M. Schmid, *J Acoust Soc Am*, 1991, **90**, 1238-1245.
76. J. J. Hawkes, W. T. Coakley, M. Groschl, E. Benes, S. Armstrong, P. J. Tasker and H. Nowotny, *J Acoust Soc Am*, 2002, **111**, 1259-1266.
77. C. Situma, M. Hashimoto and S. A. Soper, *Biomolecular Engineering*, 2006, **23**, 213-231.
78. J. Svennebring, O. Manneberg and M. Wiklund, *J Micromech Microeng*, 2007, **17**, 2469-2474.
79. M. Groschl, *Acustica*, 1998, **84**, 632-642.
80. M. Groschl, W. Burger, B. Handl, O. Doblhoff-Dier, T. Gaida and C. Schmatz, *Acta Acustica united with Acustica*, 1998, **84**, 815-822.
81. J. F. Spengler and W. T. Coakley, *Langmuir*, 2003, **19**, 3635-3642.
82. N. R. Harris, M. Hill, R. Torah, R. Townsend, S. Beeby, N. M. White and J. Ding, *Sensor Actuat a-Phys*, 2006, **132**, 311-316.
83. A. Haake, Doctoral Thesis, Technische Universität Berlin, 2004.
84. M. Groschl, *Acustica*, 1998, **84**, 432-447.
85. J. J. Shi, D. Ahmed, X. Mao and T. J. Huang, Micro Electro Mechanical Systems, 2008. MEMS 2008. IEEE 21st International Conference on, 2008.
86. C. D. Wood, S. D. Evans, J. E. Cunningham, R. O'Rorke, C. Walti and A. G. Davies, *Appl Phys Lett*, 2008, **92**, 044104
87. J. J. Hawkes and W. T. Coakley, *Sensor Actuat B-Chem*, 2001, **75**, 213-222.
88. A. Nilsson, F. Petersson, H. Jonsson and T. Laurell, *Lab Chip*, 2004, **4**, 131-135.
89. A. Lenshof, A. Ahmad-Tajudin, K. Järås, A.-M. Swärd-Nilsson, L. Åberg, G. Marko-Varga, J. Malm, H. Lilja and T. Laurell, *submitted to Analytical Chemistry*.
90. S. P. Martin, R. J. Townsend, L. A. Kuznetsova, K. A. J. Borthwick, M. Hill, M. B. McDonnell and W. T. Coakley, *Biosens Bioelectron*, 2005, **21**, 758-767.
91. H. Bruus, *Theoretical microfluidics*, Oxford University Press, Oxford, 2008.
92. K. Higashitani, M. Fukushima and Y. Matsuno, *Chemical Engineering Science*, 1981, **36**, 1877-1882.
93. H. Jonsson, C. Holm, A. Nilsson, F. Petersson, P. Johnsson and T. Laurell, *Ann Thorac Surg*, 2004, **78**, 1572-1578.
94. M. A. Sobanski, C. R. Tucker, N. E. Thomas and W. T. Coakley, *Bioseparation*, 2000, **9**, 351-357.
95. M. A. Grundy, W. E. Bolek, W. T. Coakley and E. Benes, *J Immunol Methods*, 1993, **165**, 47-57.
96. R. W. Ellis and M. A. Sobanski, *J Med Microbiol*, 2000, **49**, 853-859.

97. M. Wiklund, J. Toivonen, M. Tirri, P. Hanninen and H. M. Hertz, *J Appl Phys*, 2004, **96**, 1242-1248.
98. A. Haake, A. Neild, G. Radziwill and J. Dual, *Biotechnol Bioeng*, 2005, **92**, 8-14.
99. J. J. Hawkes, R. W. Barber, D. R. Emerson and W. T. Coakley, *Lab Chip*, 2004, **4**, 446-452.
100. P. Augustsson, J. Persson, S. Ekstrom, M. Ohlin and T. Laurell, *Lab Chip*, 2009, **9**, 810-818.
101. F. Trampler, S. A. Sonderhoff, P. W. S. Pui, D. G. Kilburn and J. M. Piret, *Bio-Technol*, 1994, **12**, 281-284.
102. P. W. S. Pui, F. Trampler, S. A. Sonderhoff, M. Groeschl, D. G. Kilburn and J. M. Piret, *Biotechnol Progr*, 1995, **11**, 146-152.
103. J. J. Hawkes and W. T. Coakley, *Enzyme Microb Tech*, 1996, **19**, 57-62.
104. K. Yasuda, S. Umemura and K. Takeda, *Jpn J Appl Phys 1*, 1995, **34**, 2715-2720.
105. J. J. Hawkes, D. Barrow and W. T. Coakley, *Ultrasonics*, 1998, **36**, 925-931.
106. N. R. Harris, M. Hill, S. Beeby, Y. Shen, N. M. White, J. J. Hawkes and W. T. Coakley, *Sensor Actuat B-Chem*, 2003, **95**, 425-434.
107. F. Petersson, A. Nilsson, C. Holm, H. Jonsson and T. Laurell, *Analyst*, 2004, **129**, 938-943.
108. F. Petersson, A. Nilsson, H. Jonsson and T. Laurell, *Anal Chem*, 2005, **77**, 1216-1221.
109. J. Persson, P. Augustsson, T. Laurell and M. Ohlin, *FEBS Journal*, 2008, **275**, 5657-5666.
110. P. Augustsson, L. Åberg, A.-M. Swärd-Nilsson and T. Laurell, *Microchimica Acta*, 2009, **164**, 269-277.
111. C. Grenvall, M. Carlsson, P. Augustsson, F. Pettersson and T. Laurell, µTAS 2007 Conference, Paris, 2007.
112. A. Lenshof, Doctoral Thesis, Lund University, 2009.
113. W. T. Coakley, D. Bazou, J. Morgan, G. A. Foster, C. W. Archer, K. Powell, K. A. J. Borthwick, C. Twomey and J. Bishop, *Colloid Surface B*, 2004, **34**, 221-230.
114. L. A. Kuznetsova, D. Bazou and W. T. Coakley, *Langmuir*, 2007, **23**, 3009-3016.
115. D. Bazou, E. J. Blain and W. T. Coakley, *Mol Membr Biol*, 2008, **25**, 102-U116.
116. D. Bazou, G. Davies, W. G. Jiang and W. T. Coakley, *Cell Commun Adhes*, 2006, **13**, 279-294.
117. J. F. Spengler, M. Jekel, K. T. Christensen, R. J. Adrian, J. J. Hawkes and W. T. Coakley, *Bioseparation*, 2000, **9**, 329-341.
118. M. Wiklund, S. Nilsson and H. M. Hertz, *J Appl Phys*, 2001, **90**, 421-426.
119. M. Wiklund, P. Spegel, S. Nilsson and H. M. Hertz, *Ultrasonics*, 2003, **41**, 329-333.

120. M. Evander, K. M. Horsman, C. J. Easley, J. P. Landers, J. Nilsson and T. Laurell, μTAS, 2006.
121. A. Neild, S. Oberti, G. Radziwill and J. Dual, *Biotechnol Bioeng*, 2007, **97**, 1335-1339.
122. A. Haake and J. Dual, *J Acoust Soc Am*, 2005, **117**, 2752-2760.
123. A. Neild, S. Oberti, A. Haake and J. Dual, *Ultrasonics*, 2006, **44**, E455-E460.
124. A. Haake and J. Dual, *Ultrasonics*, 2004, **42**, 75-80.
125. O. Manneberg, J. Svennebring, H. M. Hertz and M. Wiklund, *J Micromech Microeng*, 2008, **18**, 095025.
126. C. D. Wood, J. E. Cunningham, R. O'Rorke, C. Walti, E. H. Linfield, A. G. Davies and S. D. Evans, *Appl Phys Lett*, 2009, **94**, 054101.
127. A. Neild, S. Oberti, F. Beyeler, J. Dual and B. J. Nelson, *J Micromech Microeng*, 2006, **16**, 1562-1570.
128. G. R. Goddard, C. K. Sanders, J. C. Martin, G. Kaduchak and S. W. Graves, *Anal Chem*, 2007, **79**, 8740-8746.
129. G. Goddard and G. Kaduchak, *J Acoust Soc Am*, 2005, **117**, 3440-3447.
130. J. J. Hawkes, M. J. Long, W. T. Coakley and M. B. McDonnell, *Biosens Bioelectron*, 2004, **19**, 1021-1028.
131. K. Yasuda, K. Takeda and S. I. Umemura, *Jpn J Appl Phys 1*, 1996, **35**, 3295-3299.
132. M. Wiklund, C. Gunther, R. Lemor, M. Jager, G. Fuhr and H. M. Hertz, *Lab Chip*, 2006, **6**, 1537-1544.
133. S. K. Ravula, D. W. Branch, C. D. James, R. J. Townsend, M. Hill, G. Kaduchak, M. Ward and I. Brener, *Sensor Actuat B-Chem*, 2008, **130**, 645-652.
134. H. Y. Yu, J. W. Kwon and E. S. Kim, *J Microelectromech S*, 2006, **15**, 1015-1024.
135. O. Manneberg, B. Vanherberghen, J. Svennebring, H. M. Hertz, B. Onfelt and M. Wiklund, *Appl Phys Lett*, 2008, **93**, 063901.
136. J. Hultstrom, M. H. Hertz and M. Wiklund, 6th USWNet Conference, Zürich, 2008.
137. O. Manneberg, S. Melker Hagsäter, J. Svennebring, H. M. Hertz, J. P. Kutter, H. Bruus and M. Wiklund, *Ultrasonics*, 2009, **49**, 112-119.
138. K. Matsuda, T. Kamakura and M. Maezawa, *Japanese Journal of Applied Physics Part 1-Regular Papers Brief Communications & Review Papers*, 2006, **45**, 4448-4452.
139. O. Manneberg, J. Strååt and M. Wiklund, 6th USWNet Conferece, Zürich, 2008.
140. T. L. Tolt and D. L. Feke, *J Acoust Soc Am*, 1992, **91**, 3152-3156.
141. C. Siversson, F. Petersson, A. Nilsson and T. Laurell, The International Conference on Miniaturized Systems for Chemistry and Life Scineces, 2004.

142. M. A. H. Weiser, R. E. Apfel and E. A. Neppiras, *Acustica*, 1984, **56**, 114-119.
143. T. R. Meeker, *Publication and proposed revision of ANSI/IEEE standard 176-1987 "ANSI/IEEE standard on piezoelectricity"* 0885-3010, 1996.
144. K. Uchino and S. Hirose, *Ieee T Ultrason Ferr*, 2001, **48**, 307-321.
145. A. J. Moulson and J. M. Herbert, *Electroceramics: Materials Properties Applications*, Chapman and Hall, London, 1990.

Acta Universitatis Upsaliensis

Digital Comprehensive Summaries of Uppsala Dissertations from the Faculty of Science and Technology 641

Editor: The Dean of the Faculty of Science and Technology

A doctoral dissertation from the Faculty of Science and Technology, Uppsala University, is usually a summary of a number of papers. A few copies of the complete dissertation are kept at major Swedish research libraries, while the summary alone is distributed internationally through the series Digital Comprehensive Summaries of Uppsala Dissertations from the Faculty of Science and Technology. (Prior to January, 2005, the series was published under the title "Comprehensive Summaries of Uppsala Dissertations from the Faculty of Science and Technology".)

Distribution: publications.uu.se
urn:nbn:se:uu:diva-100758

ACTA
UNIVERSITATIS
UPSALIENSIS
UPPSALA
2009